

Analysis of crustal deformation in Luzon, Philippines using geodetic observations and earthquake focal mechanisms

Gerald Galgana^{a,b,*}, Michael Hamburger^a, Robert McCaffrey^{c,1},
Ernesto Corpuz^{d,2}, Qizhi Chen^a

^a Department of Geological Sciences, Indiana University, Bloomington, IN 47405, United States

^b Manila Observatory, Loyola Heights, Quezon City, Metro Manila, Philippines

^c Department of Earth and Environmental Sciences, Rensselaer Polytechnic Institute, Troy, NY 12180, United States

^d Philippine Institute of Volcanology and Seismology, UP Campus, Diliman, Quezon City, Philippines

Received 10 October 2006; received in revised form 30 November 2006; accepted 4 December 2006

Available online 24 January 2007

Abstract

We utilize regional GPS velocities from Luzon, Philippines, with focal mechanism data from the Harvard Centroid Moment Tensor (CMT) Catalog, to constrain tectonic deformation in the complex plate boundary zone between the Philippine Sea Plate and Eurasia (the Sundaland block). Processed satellite imagery and digital elevation models are used with existing gravity anomaly, seismicity, and geologic maps to define a suite of six elastic blocks. Geodetic and focal mechanism data are inverted simultaneously to estimate plate rotations and fault-locking parameters for each of the tectonic blocks and faults comprising Luzon. Major tectonic structures that were found to absorb the plate convergence include the Manila Trench (20–100 mm yr⁻¹) and East Luzon Trough (~9–15 mm yr⁻¹)/Philippine Trench (~29–34 mm yr⁻¹), which accommodate eastward and westward subduction beneath Luzon, respectively; the left-lateral strike-slip Philippine Fault (~20–40 mm yr⁻¹), and its northward extensions, the Northern Cordillera Fault (~17–37 mm yr⁻¹ transtension), and the Digdig Fault (~17–27 mm yr⁻¹ transpression). The Macolod Corridor, a zone of active volcanism, crustal thinning, extension, and extensive normal and strike-slip faulting in southwestern Luzon, is associated with left-lateral, transtensional slip of ~5–10 mm yr⁻¹. The Marikina Fault, which separates the Central Luzon block from the Southwestern Luzon block, reveals ~10–12 mm yr⁻¹ of left-lateral transpression. Our analysis suggests that much of the Philippine Fault and associated splays are locked to partly coupled, while the Manila and Philippine trenches appear to be poorly coupled. Luzon is best characterized as a tectonically active plate boundary zone, comprising six mobile elastic tectonic blocks between two active subduction zones. The Philippine Fault and associated intra-arc faults accommodate much of the trench-parallel component of relative plate motion.

© 2006 Elsevier B.V. All rights reserved.

Keywords: Crustal deformation; Philippines; Geodetic observations

* Corresponding author. Department of Geological Sciences, Indiana University, Bloomington, IN 47405, United States. Tel.: +1 812 855 1008, +1 812 855 2934; fax: +1 812 855 7899.

E-mail address: galgana@indiana.edu (G. Galgana).

¹ Tel.: +1 518 276 8521; fax: +1 518 276 2012.

² Tel.: +63 2 426 1468; fax: +63 2 926 7749/926 3229.

1. Introduction

Over the past several decades, a fundamental modification of the plate tectonics paradigm has taken place. The concept of rigid plates separated by discrete plate bounding faults (e.g., Morgan, 1968) has given way to a more realistic model that consists of slowly deforming, relatively rigid plates, separated by broad areas of rapid deformation, designated as plate boundary zones (e.g.,

Gordon and Stein, 1992). Plate boundary zones are of prime importance to understanding the fundamental nature of interaction between tectonic plates, as these broad zones account for the majority of the world's interplate tectonic activity (e.g., Stein and Sella, 2002; Kreemer et al., 2003). On the other hand, our understanding of plate boundary processes in these zones is challenged by the complexity and temporal variability of present-day deformation. In particular, plate boundary

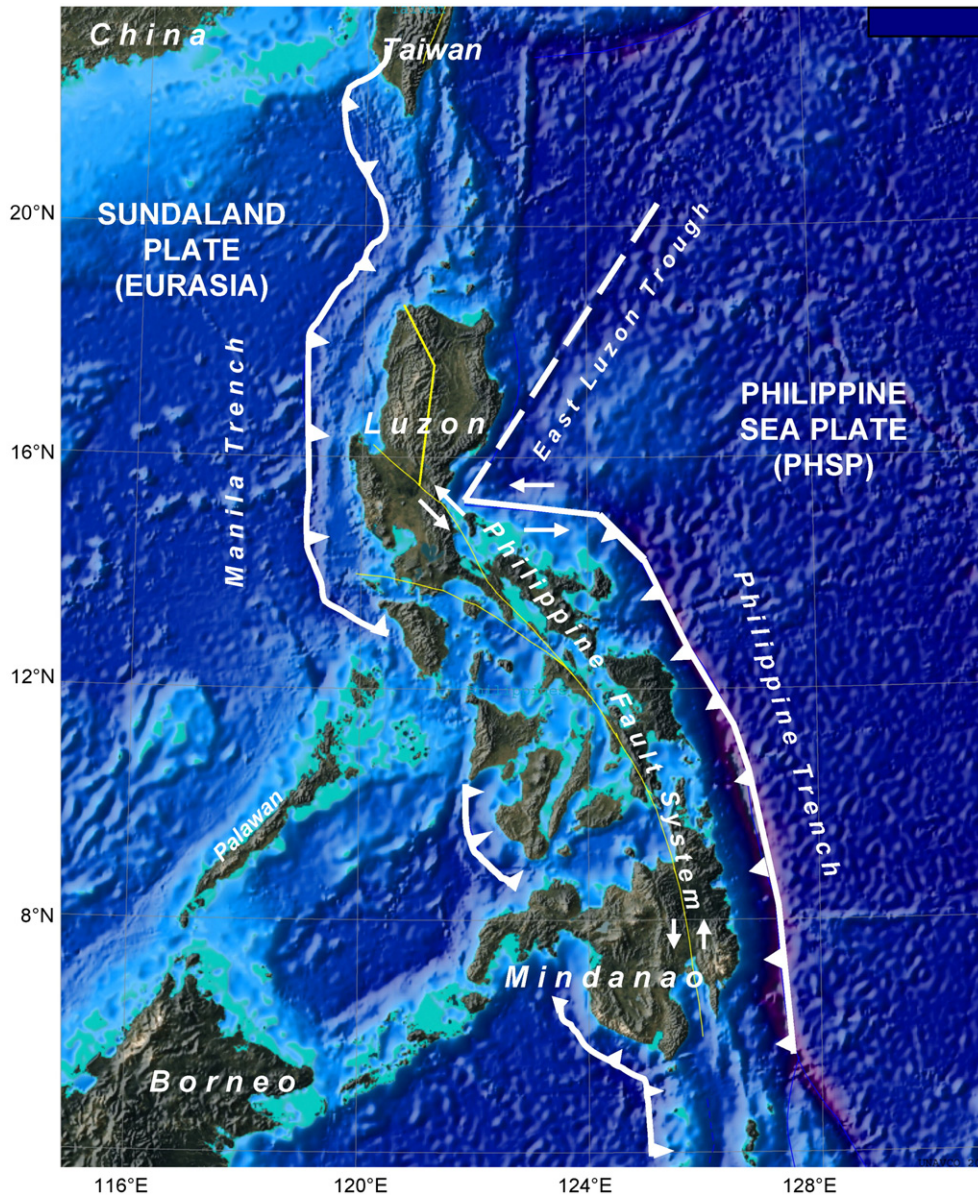


Fig. 1. Physical map of the Philippines, showing topography and bathymetry. The two opposing subduction zones (the Manila Trench and the Philippine Trench/East Luzon Trough), major plates (SUND and PHSP) and the major Philippine Fault System with splays in Luzon (yellow lines) are mapped (basemap derived from the UNAVCO Jules Verne Navigator). (For interpretation of the references to color in this figure legend, the reader is referred to the web version of this article.)

zones associated with oblique subduction (such as the Cascadia subduction zone, Sumatra in the Indonesian arc, and the North Island of New Zealand) are characterized by extensive strike-slip faulting, high seismicity, rapid vertical axis rotations and significant intraplate deformation in the overlying plate (Fitch, 1972; McCaffrey, 2002; Wallace et al., 2004). The island of Luzon, in the northern Philippine island arc, provides another example of plate boundary zone deformation. Luzon is situated in an area where the rapid convergence between the Eurasian Plate (Sundaland block) and the Philippine Sea Plate is accommodated across two major subduction zones and a rapidly deforming island arc (Fig. 1). Detailed analysis of the kinematics of Luzon will help elucidate how deformation occurs within plate boundary zones in general.

Plate boundary zones have been defined using a variety of models, ranging from a simple fault-bounded plate boundary (e.g., Morgan, 1968) to a series of sub-parallel faults and crustal blocks (e.g., Bennett et al., 1996); from half-space elastic models to more complex multi-layered elastic–viscoelastic models (e.g., Thatcher, 1995). Some models define the lithosphere as a continuously deforming viscoelastic surface (e.g., Houseman and England, 1986; Spakman and Nyst, 2003), while others define the deforming crust as a series of rotating blocks (e.g., McCaffrey, 2002). The continuous modeling approach primarily treats the lithosphere as a viscoelastic or fluid material which deforms continuously—but at variable rates—throughout the layer. The fault-and-block system describes zones of deformation as comprised of a set of finite, elastic blocks,

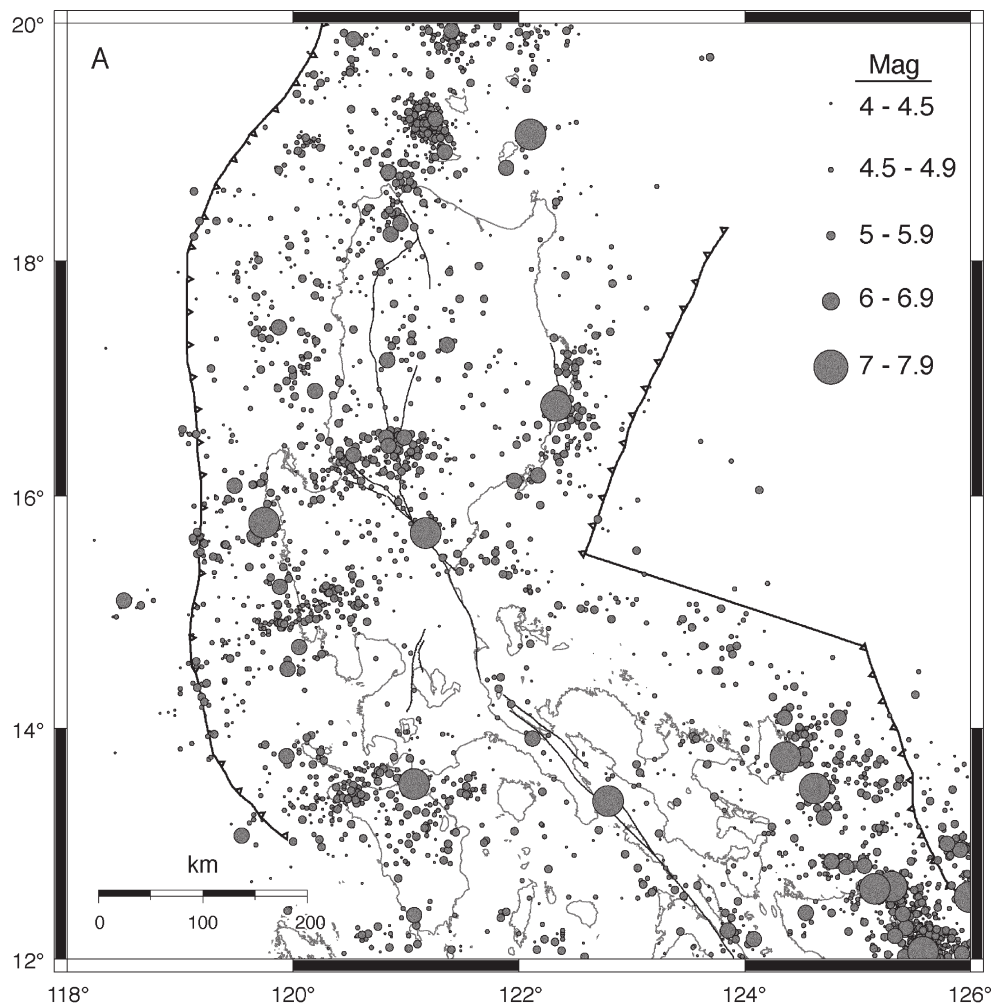


Fig. 2. A: Seismicity map (1973–2006) derived from the USGS National Earthquake Information Center (NEIC) catalogue. Magnitudes of these shallow events (depth < 70 km) are depicted by the circle diameters. B: Focal mechanism map (1977–2003) derived from the Harvard CMT Catalogue. Symbols depict lower-hemisphere projections of best double-couple solutions, with compressional quadrant shaded in black.

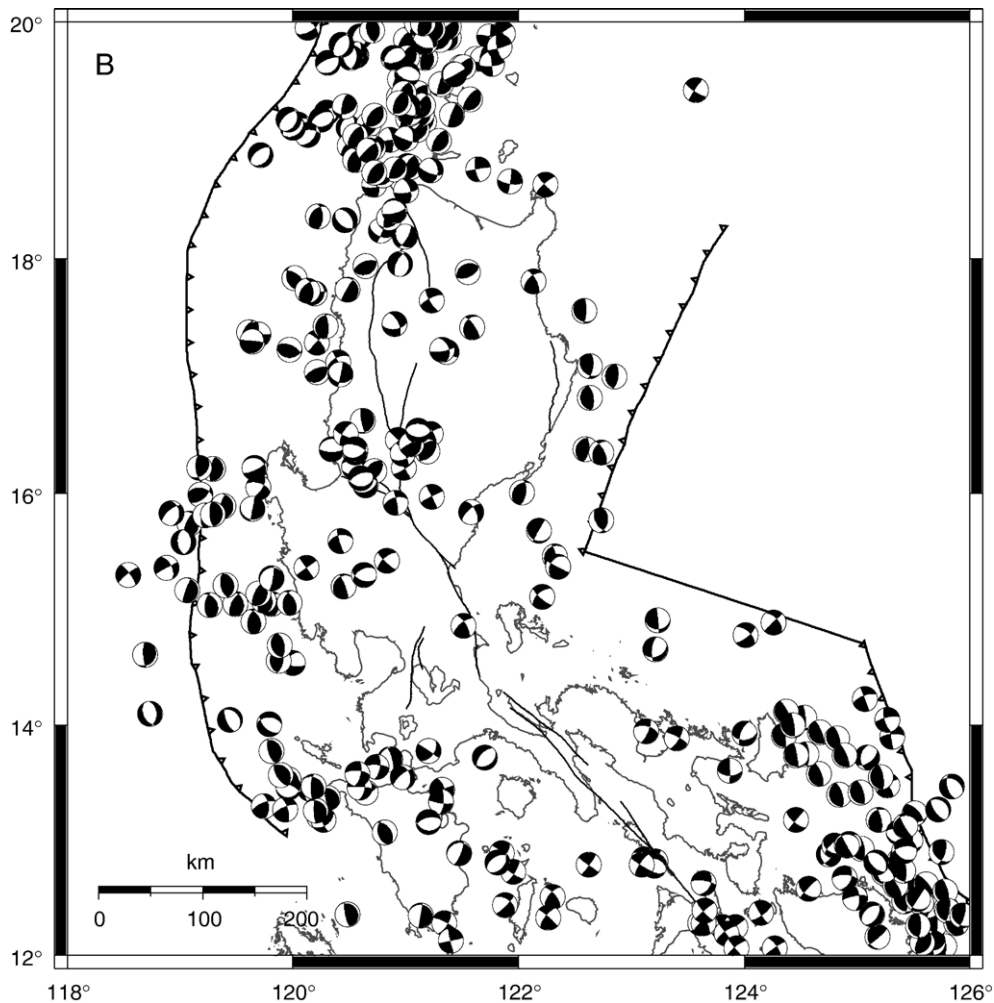


Fig. 2 (continued).

separated by discrete faults, essentially a small-scale analog to the global model of plate tectonics. While we cannot rule out the viscoelastic models of arc deformation, the presence of major, intra-arc faults within the island of Luzon, such as the Philippine Fault and Verde Passage fault system, leads us to analyze the kinematics using the finite elastic block method. In this study, we use Global Positioning System (GPS) measurements and earthquake focal mechanisms to constrain block velocities and rotations as well as estimates of slip and locking strain along major faults.

1.1. Tectonic setting

The Philippine archipelago is part of a broad zone of convergence between the Sundaland block, an independent part of Eurasian Plate (see Chamot-Rooke and Le Pichon, 1999; Michel et al., 2001) and the Philippine

Sea Plate (Fitch, 1972; Seno et al., 1993; Rangin et al., 1999). The northern Philippines is unusual in that it is characterized by opposing subduction on the east and west sides, major intra-arc strike-slip faults, active volcanism, and high seismic activity (Fig. 2) within the arc complex (Cardwell et al., 1980; Hamburger et al., 1982; Aurelio, 2000). Subduction of the Philippine Sea Plate occurs along the eastern margin of the archipelago, marked by the Philippine Trench and its northern extension, the East Luzon Trough (Fig. 1). The Philippine Trench is a seismically active, north–south trending depression characterized by a poorly defined Wadati–Benioff earthquake zone which extends to about 100 km depth (Cardwell et al., 1980). This trench, which marks the boundary of the westward-subducting Philippine Sea Plate under the Philippine Mobile Belt, extends from the Island of Mindanao in the south to its northern termination, east of central Luzon (Fig. 1). The trench is

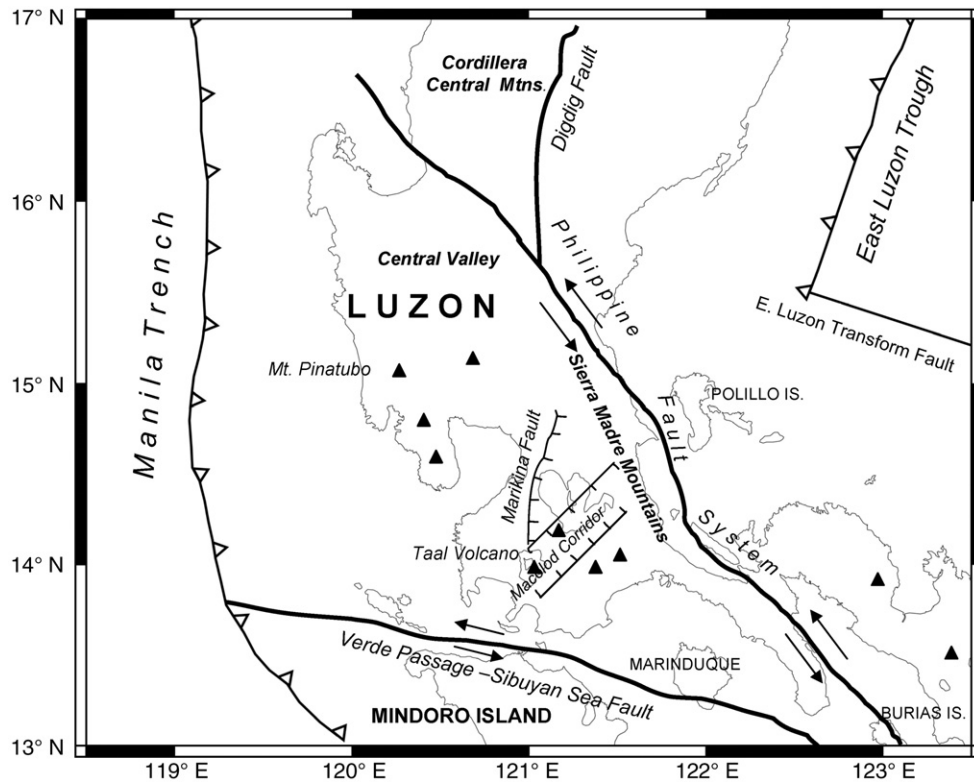


Fig. 3. Map of southwestern Luzon, showing major tectonic structures. Prominent volcanic centers are marked with triangles.

characterized by large negative gravity anomalies, and is associated with moderate to large-magnitude interplate thrust-type earthquakes (Fig. 2B) (Lewis and Hayes, 1983; Hamburger et al., 1982; Tomida, 1998). To its north, the East Luzon Trough represents a northeast-trending incipient subduction zone; it is also characterized by deep bathymetry, well-defined negative gravity anomalies, and high seismicity (Fig. 2A), but without subduction-related volcanism (Hamburger et al., 1982; Lewis and Hayes, 1983; Tomida, 1998).

On the west side of Luzon, the South China Sea Basin subducts eastward along the Manila Trench, the primary convergence zone between Eurasia and Luzon (Hayes and Lewis, 1984; Rangin et al., 1999; Yu et al., 1999). The trench is associated with a well-developed forearc system and extends southward from Taiwan in the north to Mindoro Island in the south along the western margin of Luzon (Fig. 1) (Hayes and Lewis, 1984). At its northern and southern terminations, subduction at the Manila Trench is interrupted by arc-continent collision, i.e., between the northern Philippine arc and the Eurasian continental margin at Taiwan and between the Palawan–Borneo Block and Luzon at the island of Mindoro (De Boer et al., 1980; Suppe, 1988).

Between the two subduction zones lies the seismically active, NW–SE trending, sinistral strike-slip Philippine Fault (Figs. 1 and 3) (Barrier et al., 1991; Rangin et al., 1999; Bacolcol, 2003). The Philippine Fault traverses the entire Philippine archipelago from the northeast of Mindanao Island through the central Philippines and as far north as northwestern Luzon (Fig. 1). Fault activity is estimated to have started at about 15 Ma and extends through Holocene time (Karig, 1983), although some estimates suggest a much younger age (Barrier et al., 1991). The fault divides into a series of splays across the southern Cordillera Central, where some appear to extend to the forearc region of the Manila Trench. The Philippine fault is seismically active, with fault slip rates of about 9–17 mm yr⁻¹ determined from geomorphic data (Daligdig, 1997), 20–25 mm yr⁻¹ from plate kinematics (Barrier et al., 1991), 35 mm yr⁻¹ determined from GPS measurements (Rangin et al., 1999; Yu et al., 1999; Thibault, 1999), and 68.6 mm yr⁻¹ from historical seismicity (Acharya, 1980). The fault passes through the northern mountains of the Cordillera Central, into the southern Sierra Madre mountains of east-central Luzon, and near Bondoc Peninsula in southern Luzon (Figs. 1 and 3) (Barrier

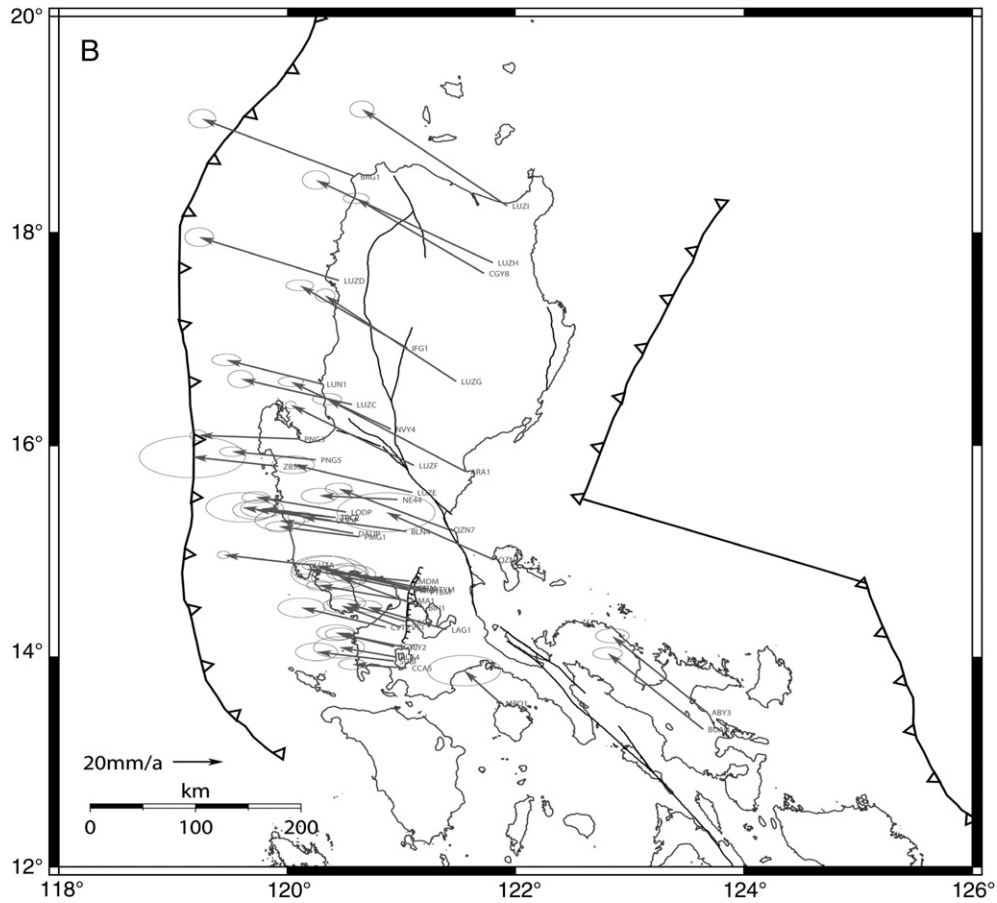


Fig. 4 (continued).

analyses (Appendix A). We used analytical hill shading to highlight the orientation of fault scarps, lineaments, and other terrain surfaces (Kennelly and Stickney, 2000; Leech et al., 2003). The approach was used to highlight surficial geologic features within Luzon, such as fault scarps of the Philippine, Northern Cordillera, Digdig, Marikina, and Macolod Corridor fault zones (Figs. 1 and 3). Bathymetric data clearly reveal the topographic structures of the Manila Trench and East Luzon Trough, as well as the Verde Passage–Sibuyan Sea Fault near southwestern Luzon (Fig. 1). Three Landsat TM scenes were used to identify faults within complex deformation areas such as the Cordillera Central (northern Luzon) and Macolod Corridor (southwestern Luzon). The addition of these visible and near-infrared reflectance data provided additional observations for determining and verifying fault scarps, lineaments, and other geologic features associated with possible present-day tectonic activity. Details of terrain and image processing/interpretation are discussed in Galgana (2005). We also inferred and cross-referenced our identified block boundaries with locations of faults and

tectonic structures based on existing literature (i.e., Förster et al., 1990; Pubellier et al., 2000, 2004; Torres et al., 2002). By combining this information with seismicity and focal mechanism data (Fig. 2A and B, respectively), the orientation and possible boundaries of the tectonic blocks that comprise Luzon can be better defined. Appendix A shows some examples of how plate boundaries were determined by analyzing the terrain models.

2.2. GPS observations

Global Positioning System (GPS) measurements have been used extensively as primary tools for geodetic observations since the late 1980s, and have proven particularly valuable for measuring plate boundary deformation and tectonic movements (e.g., Segall and Davis, 1997). The data reported here comprise repeat campaign measurements of the Luzon regional network as well as smaller sub-networks around the Marikina Fault and the active volcanoes of Taal, Pinatubo, and Mayon (Thibault, 1999; Beavan et al., 2001; Lowry

Table 1
GPS-derived velocities of campaign and continuous stations used in this study

Station name	Longitude	Latitude	V_e	V_n	Sigma_e	Sigma_n
ABY3	123.67592	13.47668	1.46	31.72	2.15	1.00
ARA1	121.56281	15.75727	-16.18	30.21	1.84	0.81
BAKO	106.84891	-6.49105	51.50	-2.33	1.58	0.76
BIN1	121.19328	14.46893	5.57	11.80	3.58	1.72
BJFS	115.89248	39.60860	10.82	140.31	1.65	0.98
BLG4	120.94863	14.00060	16.52	2.59	3.23	1.52
BLN4	121.04432	15.18999	-3.07	4.77	1.62	0.72
BRG1	120.60076	18.52034	-22.57	23.83	1.72	1.32
BUAN	123.64321	13.31098	1.07	31.64	1.88	0.85
CCA5	121.04939	13.89883	17.09	-0.10	1.69	0.78
CGY8	121.72651	17.61738	-12.37	31.33	1.65	0.72
CVT1	120.99697	14.28131	15.07	7.94	2.31	1.00
CVT2	120.86505	14.28145	5.41	7.02	3.00	1.37
DAEJ	127.37448	36.39943	61.04	-5.99	1.49	0.84
DAUP	120.58114	15.17497	9.48	4.02	3.15	1.45
IFG1	121.05154	16.92059	-4.05	25.84	1.77	0.76
LAG1	121.39818	14.26281	7.47	8.34	1.78	0.82
LAG4	121.05432	14.33302	14.60	6.67	2.44	1.07
LMDM	121.07235	14.72264	6.69	1.95	4.79	2.34
LODP	120.51712	15.37277	2.93	4.94	1.76	0.80
LUN1	120.30443	16.58256	0.65	8.93	1.84	0.82
LUZA	120.19528	14.87755	4.75	2.68	0.77	0.54
LUZC	120.56821	16.38796	-5.54	9.63	1.63	1.24
LUZD	120.45556	17.55093	-16.98	17.47	1.82	1.32
LUZE	121.09697	15.56104	-8.55	10.50	2.70	1.23
LUZF	121.11311	15.81355	-10.22	24.98	0.67	0.54
LUZG	121.48214	16.60754	-13.43	36.04	1.24	0.93
LUZH	121.80384	17.71741	-31.74	34.68	1.72	1.32
LUZI	121.92794	18.24585	-19.30	40.86	1.53	1.16
MMA1	121.03976	14.53717	4.25	5.06	1.54	0.68
MMA8	120.97271	14.59822	0.00	0.00	0.38	0.31
MRQ1	121.86888	13.56001	24.41	12.68	4.66	2.16
MTYM	121.22052	14.64136	7.34	5.94	2.67	1.25
NE44	120.96957	15.49155	7.63	0.09	2.32	1.06
NTUS	103.67996	1.34580	63.68	-1.58	5.36	2.25
NVY4	120.90746	16.15877	-0.97	19.17	1.60	0.70
PIMO	121.07773	14.63572	-2.05	7.70	1.63	0.74
PIVS	121.05873	14.65219	2.02	8.38	1.63	0.72
PMG1	120.63321	15.14022	6.69	2.82	1.65	0.73
PNG3	120.10790	16.06330	-1.44	0.00	1.05	0.78
PNG5	120.25369	15.86768	5.33	2.01	1.56	0.69
PTBM	121.20801	14.62012	10.68	5.98	2.74	1.29
QZN3	121.80678	14.92528	-3.78	19.12	6.24	2.76
QZN7	121.41497	15.21113	-4.86	16.31	1.70	0.76
SHAO	121.20044	31.09964	63.19	-7.63	1.41	0.67
SUBI	120.93997	13.96205	8.01	2.39	2.68	1.25
SUWN	127.05424	37.27552	58.89	-5.66	1.44	0.76
TGYT	120.93926	14.09765	15.57	4.55	2.42	1.12
TLY2	121.02194	14.09566	13.41	4.15	1.81	0.84
TRC2	120.42575	15.32313	6.75	1.70	2.84	1.32
TRCP	120.42239	15.32424	9.68	2.30	2.74	1.27
UODP	120.38702	15.29706	3.42	4.07	4.62	2.09
UPHM	121.05970	14.65527	5.22	6.71	4.05	1.89
WUHN	114.35726	30.53165	61.91	-5.52	1.38	0.63
XIAN	109.22149	34.36867	61.06	-7.22	1.65	0.98
ZBS3	119.92470	15.80569	4.44	2.54	6.73	2.94
ZBS9	120.06370	15.03094	-9.73	10.88	10.09	4.40

et al., 2001; Bartel, 2002; Bartel et al., 2003). The entire Luzon GPS network is composed of 52 stations (Fig. 4A and B), most of which were selected from monuments of the Philippine GPS Reference System (established in 1992). These survey points were occupied using dual-frequency, survey-grade receivers through campaign-style observations in 1996, 1998, 1999 and 2002. These campaign stations were linked through observations from continuous GPS stations PIMO and MMA8, both situated in Metro Manila (Table 1). Processing of these campaign data was initially completed by Thibault (1999) and Bartel (2002), using the BERNESE software (Rothacher and Mervart, 1996). We undertook processing of the recent 2002 dataset, as well as reprocessing of the 1996–99 GPS data using the NASA-JPL GIPSY-OASIS II software (Webb and Zumberge, 1993).

The processing approach involved conventional analysis of both campaign and continuous GPS data in a consistent reference frame to determine site positions and velocities. Raw GPS data collected in the field were analyzed in 24-hour daily solutions along with regional and global permanent sites. For the campaign GPS data, our regional solutions were determined by combining campaign data with a regional set of permanent sites and used fixed orbits and satellite clock corrections provided by JPL. The daily free network solutions were transformed into the ITRF1997 reference frame (International Terrestrial Reference Frame, epoch 1997) by estimating a seven-parameter similarity transformation for each solution (Boucher et al., 1999). Finally, individual daily GPS solutions were combined to determine site velocities. The coordinates in the ITRF1997 reference frame and their covariance matrix from the daily GPS solutions were used in a standard weighted least-squares fit to estimate site positions at a fixed epoch and site velocities. The input covariances were then scaled by a factor, so that the reduced χ^2 statistic is equal to 1.0, thus assuming a Gaussian error distribution. This approach, while in reality underestimates true error conditions, assumes that blunders and significant errors have been removed from the GPS observations through periodic campaign-style measurements and by selectively removing sites affected by local (i.e., cultural and volcanic) deformation. This strategy has been used successfully to interpret GPS observations in both large-scale (Larson et al., 1997; Wang et al., 2001) and regional networks (Freymueller et al., 1999, 2000). The extension of campaign observations through 2002,

combined with systematic reprocessing of GPS campaign data resulted in higher accuracies of GPS velocities.

The observed GPS velocity field (Fig. 4A, and Table 1), shown in a reference frame with station MMA8 in Manila fixed, provides evidence for significant intra-arc deformation. The horizontal velocity field indicates NNW-trending relative motion at rates of $\sim 35\text{--}45\text{ mm yr}^{-1}$ in northeastern Luzon, presumably a result of shear along the Philippine Fault, while site velocities in northwestern Luzon side display a more northwesterly-oriented motion at slightly reduced rates. This contrasting motion probably results from variable slip along the northern splays of the Philippine Fault (Fig. 4A and B). The observed motion in southeastern Luzon indicates an almost northerly trend with rates of $\sim 35\text{ mm yr}^{-1}$, again the result of shear along the central Philippine Fault, while stations in southwestern Luzon show east- and north-trending velocities at rates of $\sim 4\text{--}10\text{ mm yr}^{-1}$ presumably associated with relatively slow deformation along the Macolod Corridor. Sites within central Luzon near the Philippine Fault show northwest-trending velocities at $\sim 20\text{--}30\text{ mm yr}^{-1}$. This reduced velocity results from elastic deformation associated with coupling along locked segments of the Philippine Fault.

2.3. Slip vectors from earthquake focal mechanisms

Earthquake focal mechanism data provide directional constraints on present-day fault motion in Luzon. In this study, we use centroid moment tensor (CMT) earthquake mechanism data from the Harvard CMT Catalog (Dziewonski et al., 1981; Dziewonski and Woodhouse, 1983). Together with epicenter maps (Fig. 2A), slip azimuth data from these focal mechanisms can be used to define which tectonic structures are active, as well as the kinematics of motion occurring along these structures. The CMT solutions (Fig. 2B) show systematic patterns associated with the major plate and block boundaries identified in this study. We observe relatively uniform, west-oriented thrust mechanisms along the eastern margin of Luzon, near the Philippine Trench and the East Luzon Trough, consistent with the westward sense of subduction of the Philippine Sea Plate. Along the western Luzon coast, near the Manila Trench, opposing east-oriented thrust mechanisms are present, consistent with the

Notes to Table 1:

Velocities are based on campaign observations made from 1996 to 2002, using datasets from the Luzon network and the stations of Yu et al. (1999). Reference is MMA8, located in CLUZ. $V_n\text{--}V_e$ correlation is close to zero.

subduction of the South China Sea crust under northern Luzon. Strike-slip focal mechanisms are prevalent in the central Luzon area near the Philippine Fault, as well as at the southern Luzon coast, near the Verde Passage–Sibuyan Sea Fault, with fault planes subparallel to those two structures. Along the southwestern Luzon coast, thrust mechanisms are rotated to a NE–SW orientation, presumably a result of the Palawan–Mindoro block collision. Areas offshore northwestern Luzon show generally SSE-trending thrust mechanisms with some strike-slip mechanisms located near the Digdig Fault. A complex area of deformation, including normal, thrust, and shear mechanisms, occupies the Luzon Strait between Luzon and Taiwan. While recognizing that there are other intra-block earthquake mechanisms within Luzon, we favored to select and use events that would help constrain deformation along the eastern and western subduction zones as well as the major boundaries such as the Philippine Fault and the southern Verde Passage–Sibuyan Sea Fault. The rather sparse geodetic coverage in some areas (e.g. ILOC, BBLK) prevents high resolution tectonic analysis; in this case we can use prominent focal mechanism trends in order to make a reasonable first-order approximation of block motions.

2.4. Poles of rotation

Euler poles of rotation were initially defined for the major plates based on Seno et al. (1993) (Philippine Sea Plate and Eurasia), Chamot-Rooke and Le Pichon (1999) (Eurasia and Sundaland) and Rangin et al. (1999) (Sundaland–Ilocos–Philippine Sea Plate). Subsequent inversions are made in order to refine estimates of Euler poles and rotation rates, both for major plates and smaller blocks comprising Luzon. Initial plate rotation models are shown in Table 2.

Table 2
Initial values of Euler poles used in this study

Plate pairs	Latitude	Longitude	Rate (°/My) [ccw is +]	Reference
EURA– PHSP	48.23°N	156.97°E	1.038	Seno et al. (1993)
SUND– EURA	33.23°S	129.80°E	–0.286	Chamot-Rooke and Le Pichon (1999)
ILOC– SUND	9.34°N	118.29°E	5.478	Rangin et al. (1999)
ILOC– PHSP	17.60°N	122.10°E	6.000	Rangin et al. (1999)

EURA = Eurasian Plate, SUND = Sundaland plate, ILOC = Ilocos Block, Northern Luzon and PHSP = Philippine Sea Plate.

3. Modeling method

We model crustal deformation of Luzon using the elastic block approach. This model considers the lithosphere of an actively deforming zone to be composed of a series of finite elastic blocks bounded by faults. The faults are defined in 3D space by a series of along-strike nodes, whose spacing depends on the fault complexity, and downdip nodes, designated from 10 km depth to 25 km depth. For subduction zones, these nodes extend to 50 km depth, based on seismicity data. Then, using GPS site velocities and earthquake slip vectors as observed data, we simultaneously invert for block rotation and fault-locking parameters. Relative block motion is quantified by angular velocities (Euler poles and rotation rates) that in turn define fault slip vectors as a function of position along the fault. The forward model of predicted surface deformation due to fault locking is calculated using an elastic, half-space dislocation model (Okada, 1985). This fault-locking strain is calculated by integration of surface deformation produced by fault slip over small, finite fault patches between the nodes, with bilinear interpolation used for estimating slip magnitude and coupling values at every patch (program DEFNODE (McCaffrey, 1995, 2002)).

Frictional locking along faults produces strain in the adjacent rocks, a deformation which counteracts free translation of the blocks relative to neighboring blocks. Fault locking along the faults is parameterized using fault coupling values (φ) assigned or estimated at every node, with $\varphi = 1$ representing 100% coupling and $\varphi = 0$ representing 0% coupling (i.e., fully creeping). The coupling ratio (φ) is mainly a kinematic variable defined as $\varphi = 1 - V_c/V$, where V_c is the short-term displacement rate along the fault and V is the long-term slip rate (Wallace et al., 2004).

3.1. Block identification

Block boundaries were delineated through analysis of bathymetry and topography, correlated with geologic and tectonic maps, seismicity, focal mechanisms, and gravity anomalies. Block boundaries are identified by areas of sharp discontinuities in rock formations, strong gradients in gravity or magnetic properties, discontinuities in seismic profiles, gradients in topography and bathymetry, fault scarps, prominent ground fractures and lineations, topographic depressions, uplifted blocks or seismicity. In addition, GPS velocities aid in selecting the tectonic blocks by identifying apparent groupings of the velocities based on orientations and rates. The

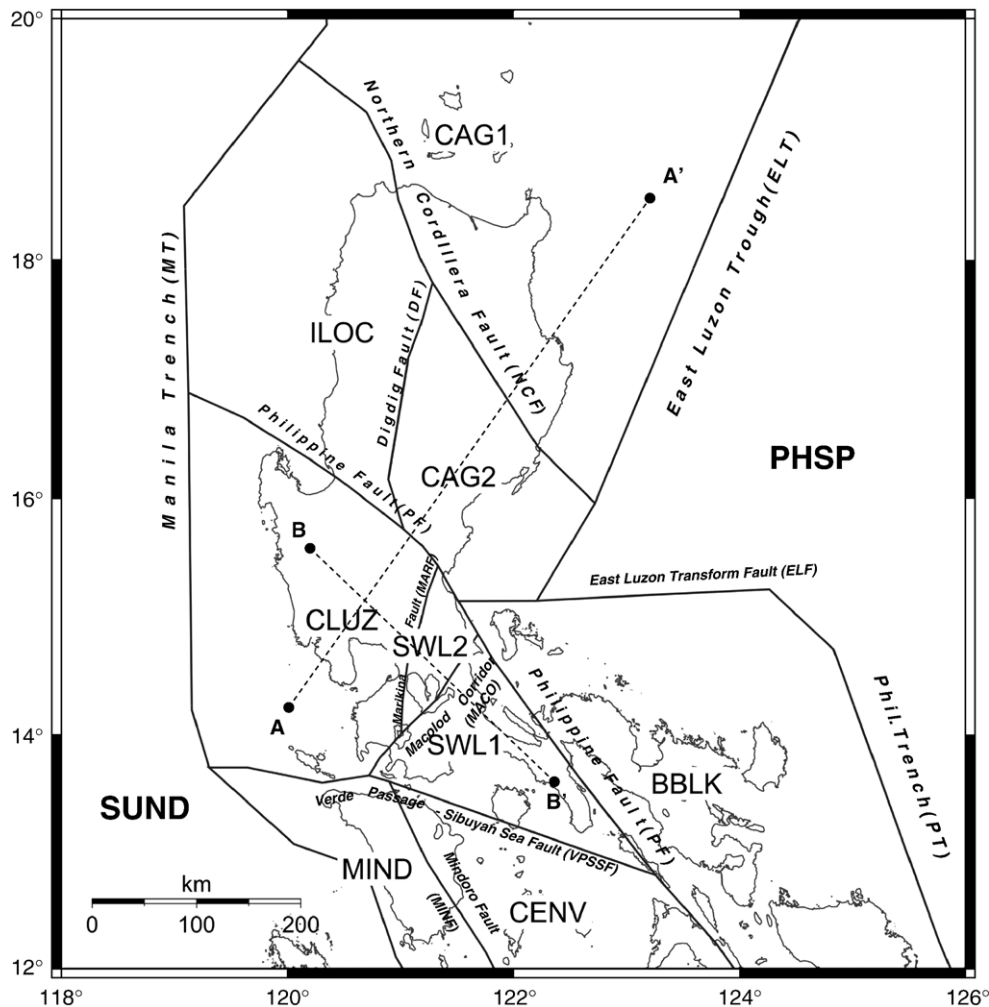


Fig. 5. Microplate map of Luzon. Seven blocks were initially assigned to comprise Luzon, designated as the following: Central Luzon (CLUZ), Southwestern Luzon 1 and 2 (SWL1, SWL2), Northwestern Luzon or Ilocos (ILOC), Northeastern Luzon or Cagayan 1 (CAG1), Cagayan 2 (CAG2), and Southeastern Luzon or Bicol (BBLK). Mindoro (MIND) and Central Visayas (CENV) were added as adjoining southern blocks, while Eurasia (EUR), Sundaland (SUND), and the Philippine Sea Plate (PHSP) were the major plates near the PMB. Section lines A–A' and B–B' cross the Philippine Fault, and the Marikina Fault–Macolod Corridor, respectively. See details on Figs. 10 and 12.

velocities are grouped together based on uniform motion, separated from those with significant gradients of velocity magnitude and/or orientation.

Seven blocks were initially defined to comprise Luzon, as shown in Fig. 5: Central Luzon (CLUZ), eastern and western blocks of Southwestern Luzon (SWL1, SWL2), Ilocos (ILOC), Northern Cagayan (CAG1), Southern Cagayan (CAG2), and Southeastern Luzon or Bicol (BBLK). Two adjacent southern blocks were added (Mindoro or MIND and Central Visayas or CENV) to create a more accurate southern Luzon boundary. Three major plates were used to describe regional motions: Eurasia (EUR), the Philippine Sea

Plate (PHSP), and Sundaland or SUND (Chamot-Rooke and Le Pichon, 1999). The blocks are separated by the following faults and subduction zones (Fig. 5): The Manila Trench (MT), the East Luzon Trough (ELT), the Philippine Trench (PT), Philippine Fault (PF-N, PF-M, and PF-S), Verde Passage–Sibuyan Sea Fault (VPSSF1 and VPSSF2), Macolod Corridor (MACO), Marikina Fault (MARF), Digdig Fault (DF), East Luzon Transform Fault (ELF) and the Northern Cordillera Fault (NCF). The modeling approach described above predicts fault slip rates on each of these block boundaries. While we recognize that some blocks exhibit possible significant internal deformation as depicted by

seismicity and numerous focal mechanisms (e.g., ILOC and BBLK), the density of our GPS sites in some locations prevents higher resolution analysis. Hence the described blocks represent a first-order approximation of the Luzon region.

3.2. Block models

Initially, we ran a series of tests to infer the physical arrangements of tectonic plates. Models were run, for instance, to verify the hypothesis that Luzon moves relative to both Sundaland and the Philippine Sea Plate (see discussion in Beavan et al., 2001), or whether it could be described as a relatively simple two-plate system based on a single dominant NW–SE Philippine Fault, in addition to the east and west subduction zones (Barrier et al., 1991; Bartel, 2002). Progressively more complex combinations such as a three-plate system involving a splaying Philippine Fault (Thibault, 1999) or four-, five-, six-, and seven-plate systems were examined. The best-fit model is determined through minimization of misfit between 57 observed and predicted velocity vectors and 78 focal mechanism slip vectors. This misfit is parameterized as the reduced chi-square value (total chi-square divided by the degree of freedom):

$$\chi_r^2 = \frac{\sum_{i=1,n} (r_i/\sigma_i)^2}{n-m}, \quad (1)$$

where n is the number of observations; m is the number of free parameters; r_i is the residual associated with each observation (or observed minus calculated velocity), and σ_i is the data uncertainty. Minimization is done using simulated annealing with a downhill simplex method (McCaffrey, 2002). For the various models, data misfit is tested using this reduced chi-square (χ_r^2) statistic. Chi-square values for the various models are compared, with the resulting lowest value representing the best fit between observed and predicted values. A χ_r^2 value much greater than 1 indicates a relatively poor fit for the current model, while a value close to 1 indicates acceptable model fit. We then apply F -tests to determine whether improvements in resulting χ^2 are statistically significant. F -tests are used to compare variances of distributions, and compare results of two models with varying parameters (e.g., Stein and Gordon, 1984). Probabilities of having one model being statistically different from another, and not entirely due to random variability within a population, are determined through the resulting F -tests.

4. Results

4.1. General strategy of tests

We devised a hierarchy of tests that move from simple to progressively more complex models of explaining present-day crustal deformation in Luzon. First, we examined whether deformation in Luzon could be explained by a single block or by simple combinations of two tectonic blocks attached to either the Sundaland Plate or the Philippine Sea Plate. Then, we addressed whether the kinematics of Luzon could be explained by block rotations alone or a combination of both block rotations and fault strain is needed. We then explored models in which Luzon could be composed of two, three, or more tectonic blocks. Next, we tested for coupling along faults by fixing locking values along fault planes, or by allowing the program to solve for the coupling value. We also investigated the locking depths of active faults by examining models with variable coupling as a function of depth.

4.2. Tests for block independence

To test for block independence, we solved for Luzon initially as one solitary block, then as a block attached to either the Sundaland Plate or the Philippine Sea Plate. As a second test, Luzon was made a two-block system, with the northeastern block associated with the Philippine Sea Plate, and the southwestern block associated with the Sundaland Plate. Model EG21, which allowed for uniform internal strain on a single Luzon block, produced a poor fit; $\chi_r^2=6.92$ (Table 3). Models considering Luzon as part of PHSP (EG40) or SUND (EG41) produced higher misfits: $\chi_r^2=36.66$ and $\chi_r^2=12.78$, respectively. Model EG42 that partitioned Luzon into two blocks with the Philippine Fault as the main locus of motion produced a poor fit: $\chi_r^2=33.77$. This model attaches the southwest side of Luzon (ILOC, SWL1, SWL2, CLUZ, MIND, CENV) to SUND and the northwest side of Luzon (CAG1, CAG2, BBLK) to PHSP.

Tests were run to evaluate the contributions of rotation and coupling, by comparing the block rotation-only model (no fault coupling) versus the block rotation with fault coupling model. For the no-elastic strain (block rotation-only) model, EG33 (7 blocks in this case), $\chi_r^2=7.42$ was obtained, as opposed to $\chi_r^2=8.33$ for EG15, the model which considered only one pole of rotation for Luzon, plus elastic strain associated with coupling along the three subduction zones (i.e., MT, ELT, and PT; see Table 3). The result indicates that block rotation, in addition to the elastic strain along

Table 3
Summary of model chi-square values and *F*-tests for block independence

Model	Description	No. of data	No. of parameters	DOF	Total χ^2	Reduced χ^2	Prob. (%)
EG40 (1 block)	Luzon is 1 block, part of PHSP	186	19	167	6121.88	36.66	0
EG41 (1 block)	Luzon is 1 block, part of SUND	186	19	167	2134.93	12.78	0
EG42 (2 blocks)	Luzon 2 parts: SW Luzon part of SUND, NE Luzon part of PHSP	186	28	158	5335.10	33.77	0
EG21 (1 block)	Luzon is 1 block, with internal strain	186	26	160	1106.72	6.92	0
EG33 (7 blocks)	Rotation only	186	33	153	1135.04	7.42	0
EG15 (1 block)	Fault coupling only	186	23	163	1358.03	8.33	0
EG20 (7 blocks)	Without earthquake slip vectors; with rotation and coupling	108	46	62	153.45	2.48	99.7
EG53 (1 block)	Poles of rotation fixed for EURA, PHSP, SUND	186	40	146	379.32	2.60	4.57
EG01 (7 Luzon blocks)	With earthquake slip vectors, rotation and locking	186	46	140	313.26	2.24	–

The probability (Prob.) column indicates the degree to which the current model is statistically similar to the best-fit model (EG01 in this case). Model names are designated arbitrarily. DOF=Degrees of Freedom.

subduction zones, is required to explain deformation within Luzon. A model using combined rotations and elastic strain provided a significantly more accurate representation of the regional kinematics, with $\chi_r^2=2.24$ (seven-block model EG01). *F*-tests demonstrate that this model is statistically distinguishable from the other previously described models (Table 3). The results show that while block rotations can explain the majority of the regional deformation in Luzon, fault-locking strain still makes a significant contribution to the observed GPS velocity field.

Tests on models were also run using only GPS velocities as input, earthquake slip vectors only, and combined GPS and slip vector data. Tests using only GPS velocities (i.e., without earthquake slip vectors) for combined fault coupling and rotation produced models with a nearly equivalent fit at $\chi_r^2=2.47$ (EG20); since this model has fewer constraints as the directions of block motions are not constrained by earthquake slip, we elected to include earthquake slip vectors as observational constraints in all further tests (e.g., EG01).

Through the results of these initial sensitivity tests, we verified that crustal deformation in Luzon is best approached by models which considered a combination of block rotations, fault coupling, and elastic strain, and

those which included both GPS data and earthquake slip vectors. These tests demonstrated that Luzon is part of neither SUND nor PHSP. Nor could Luzon be explained as an overlying solitary plate between SUND and PHSP. These findings indicate that active deformation is indeed occurring across the entire arc complex with the system of crustal faults contributing to the process. The succeeding sensitivity tests delve further into the details of a multi-block system of deformation in the northern Philippines.

4.3. Block model tests

To find an optimal block model for Luzon, an additional set of inversions were run. Chi-square values were obtained and sensitivity *F*-tests were made between the full seven-block model versus the two, three, four, five, and six-block models. These sets of tests were conducted to determine whether the fit improves statistically upon considering successively larger numbers of blocks.

With the results of inversions from these given block models, it is noted that a systematic decrease (until the 7-block model) in χ_r^2 was evident as the number of blocks is increased. The minimum reduced chi-square

Table 4
Summary of chi-square values and *F*-tests conducted for varying the numbers of blocks comprising Luzon, with both fault locking and block rotations considered in the inversion

Model	Description	No. of data	No. of parameters	DOF	Total χ^2	Reduced χ^2	Prob. (%)
EG11	Two-block model	186	30	156	400.24	2.57	2.1
EG12	Three-block model	186	33	153	348.31	2.28	11.8
EG13	Four-block model	186	36	150	370.87	2.47	5.9
EG32	Five-block model	186	40	146	331.96	2.27	18.8
EH02	Six-block model	186	40	146	286.57	1.96	–
EG01	Seven-block model	186	46	140	313.26	2.24	29.7

The probability (Prob.) column indicates the degree to which the current model is statistically similar to the best-fit model EH02.

Table 5

Summary of chi-square values and F -tests on models with various coupling parameters of faults and subduction zones bounding the blocks

Model	Description	No. of data	No. of parameters	DOF	Total χ^2	Reduced χ^2	Prob. (%)
EH02	Variable coupling	186	40	146	286.57	1.96	–
EG74	Fully coupled	186	33	153	494.46	3.23	0.05
EJ20	Coupling at 1, 0.5, 0	186	27	159	556.48	3.50	0.003
EJ21	Coupling forced to 0 for bottom nodes, top nodes variable	186	53	133	347.68	2.61	12.68

The probability (Prob.) column indicates the degree to which the current model is statistically similar to the best-fit model EH02.

value was associated with EH02, meaning that block motions are best modeled as a product of six moving blocks. F -tests comparing EH02 with the other models in this set of tests also confirm that it is statistically distinct from the other models (Table 4). Hence, we conclude that motion along several faults within Luzon contributes to the active crustal deformation of the area. We infer, however, that the fault separating blocks CAG1 and CAG2 can be neglected, given the comparison of results for the seven-block model (EG01) against the six-block model (EH02).

4.4. Coupling tests

In another series of tests, we modified coupling values, ranging from fixing the coupling parameter (φ) or solving for the φ value (making it variable from being locked or 1 and fully uncoupled or 0). These tests were designed to verify how tectonic motion is accommodated, and to what depths elastic strain extends. Furthermore, the coupling tests provide evidence of elastic strain accumulation rates, and in turn, possible indications of slip deficits and seismic potential for faults. These tests fix the top, middle, and bottom nodes to values of $\varphi = 1.0$ (locked), 0.5 (50% partly coupled), and 0 (fully uncoupled). Other tests involved solving for the top and middle nodes, while fixing the bottom nodes with zero coupling. Coupling along the subduction interfaces (MT, PT, ELT) and other faults are tested by either partially coupling or locking the plate boundaries. The

coupling or φ value is forced to decrease monotonically downdip, as plate coupling theoretically reduces to zero at depth (McCaffrey, 2002). Test results eventually showed that the variable coupling model was statistically better and significantly different than both the fully coupled model and the fixed coupling model (Table 5). Coupling for certain faults and subduction zones (e.g., the Eastern Verde Passage–Sibuyan Sea Fault, the southern Philippine Fault and the East Luzon Trough), however, resulted in high uncertainties due to lack of adequate constraints, principally a paucity of near-field geodetic observations.

4.5. Tests for locking depth

In the tests summarized in Table 6, the best-fit model is subjected to variations in locking depth of the Philippine Fault system. The locking depth was varied from 15, 20, 25, 30 and 35 km by applying variable coupling values as a function of depth. Results in Table 6 show that a 25-km locking depth gives the best fit. This result is consistent with the 20–25 km coseismic rupture estimates of Silcock and Beavan (2001) and the July 16, 1990 earthquake hypocenter depth of 25 km (Beavan et al., 2001) along the Philippine Fault.

Based on this suite of model tests, which verified a range of block combinations, fault-locking depth, and coupling parameters, we conclude that the best representation of crustal deformation for the island of Luzon is a model comprised of six elastic blocks (model

Table 6

Summary of chi-square values and F -tests on models with different average locking depths of the faults and subduction zones bounding the Luzon blocks

Model	Description	No. of data	No. of parameters	DOF	Total χ^2	Reduced χ^2	Prob. (%)
EG74	15 km locking depth	186	46	140	355.71	2.54	9.84
EG57	20 km locking depth	186	46	140	330.39	2.36	19.81
EH02	25 km locking depth	186	40	146	286.57	1.96	–
EJ31	30 km locking depth	186	40	146	388.47	2.66	3.35
EJ32	35 km locking depth	186	40	146	339.04	2.32	15.54

The probability (Prob.) column indicates the degree to which the current model is statistically similar to the best-fit model EH02.

EH02). This model includes both rotations and fault locking with variable coupling for all the faults (along strike and with depth), to a 25 km locking depth.

5. Discussion

Our newly obtained surface velocity field and published earthquake source mechanisms provide new constraints on the nature of present-day deformation in a complex plate boundary zone. In general, our preferred model describes Luzon as an actively deforming island arc, bounded by subduction zones on its flanks and internally divided into discrete blocks by active intra-arc faults. Deformation along the margins of Luzon is dominated by arc-normal convergence, while intra-arc deformation is dominated by arc-parallel deformation. The oblique convergence between the Eurasian and Philippine Sea plates is accommodated through a combination of predominantly shear deformation within and around Luzon: left-lateral strike-slip motion along the Philippine Fault, left-lateral strike-slip motion along the Verde Passage–Sibuyan Sea Fault, deformation

along the Macolod Corridor and Marikina Fault, transpression along the Digidig Fault, and transtensional motion along the Northern Cordillera Fault (Table 7). This partitioning of oblique convergence into arc-normal and arc-parallel components was first described in the Philippines (Fitch, 1972), and has been confirmed by numerous subsequent investigations (Cardwell et al., 1980; Hamburger et al., 1982; Barrier et al., 1991; Aurelio, 2000). This strain partitioning process appears to be typical of oblique subduction along many convergent plate zones (McCaffrey, 1992).

5.1. General pattern of deformation in Luzon

The details of active crustal deformation for the Luzon area are graphically depicted in Figs. 4–7, for our preferred model EH02. The GPS vectors (Fig. 6) show a close match between observed and predicted velocities. We note, however, that discrepancies exist in some stations such as MRQ1 (Marinduque Island, south of Luzon), presumably because of discrepancies between earthquake slip vectors and the single geodetic constraint in block SW Luzon 1. Sites in very close proximity to faults, such as IFG1 near the Digidig Fault and QZN1 and QZN2 near the Philippine Fault, show significant discrepancies in both magnitude and orientation, presumably associated with unmodeled deformation in the near-field of these major fault zones.

The modeled block velocity patterns (Fig. 8) show the combination of both convergence with the major plates flanking Luzon and significant internal deformation of the northern Philippine arc. We conclude that PHSP is converging with Luzon at rates of 28–39 mm yr⁻¹ in a northwesterly direction, while the convergence between SUND and central Luzon is highly variable, at rates ranging from 20 to 100 mm yr⁻¹. Slip along the Manila Trench appears to reach its maximum at ~100 mm yr⁻¹ at its northern extremity (near 19.7°N), decreasing gradually to ~50 mm yr⁻¹ in central Luzon (at the SUND–CLUZ boundary, near 16°N). Further south, along the SUND–MIND boundary, the slip appears to drop significantly, to around 20 mm yr⁻¹, presumably a result of the Palawan–Mindoro collision at the southern termination of the Manila Trench (Fig. 2). Our model also documents westward convergence along the Philippine Trench (29–34 mm yr⁻¹) and at the East Luzon Trough (95 mm yr⁻¹), though at a significantly smaller rate. Based on our results, the principal locus of plate convergence (about 60–70%) occurs at the Manila Trench, rather than at the eastern subduction zones (Table 7). This is consistent with the conclusions of Kreemer et al. (2000).

Table 7
Summary of fault and subduction slip rates based on the best-fit model, EH02

Fault/subduction zone name	Slip rate estimates (mm/yr ⁻¹)	Sense of motion
Digidig Fault	17±9 to 27±10	Transpression, oblique sinistral strike-slip
Macolod Corridor	5±11 to 10±11	Transtensional motion
Marikina Fault	10±11 to 12±11	Transpression, sinistral strike-slip
East Luzon Transform Fault	28±12 to 39±8	Sinistral strike-slip
Philippine Trench	29±10 to 34±13	Westward subduction
East Luzon Trough	9±6 to 15±7	Westward subduction
Manila Trench	20±16 to 100±16	Eastward subduction
Phil. Fault-South (BBLK–SWL1)	29±16 to 25±14	Sinistral strike-slip
Phil. Fault-Middle (CLUZ–CAG2, SWL2–BBLK)	29±11 to 40±9	Sinistral strike-slip
Phil. Fault-North (ILOC–CLUZ)	10±9 to 15±10	Sinistral strike-slip
Verde Passage–Sibuyan Sea Fault 1 (MIND–CLUZ)	39±24 to 41±20	Sinistral strike-slip
Verde Passage–Sibuyan Sea Fault 2 (CENV–SWL1)	39±24 to 41±20	Sinistral strike-slip
Northern Cordillera Fault	17±9 to 37±12	Transtensional motion

The values indicate the range (minimum and maximum) of fault slip rates within the fault, considering all nodes from both strike and dip direction.

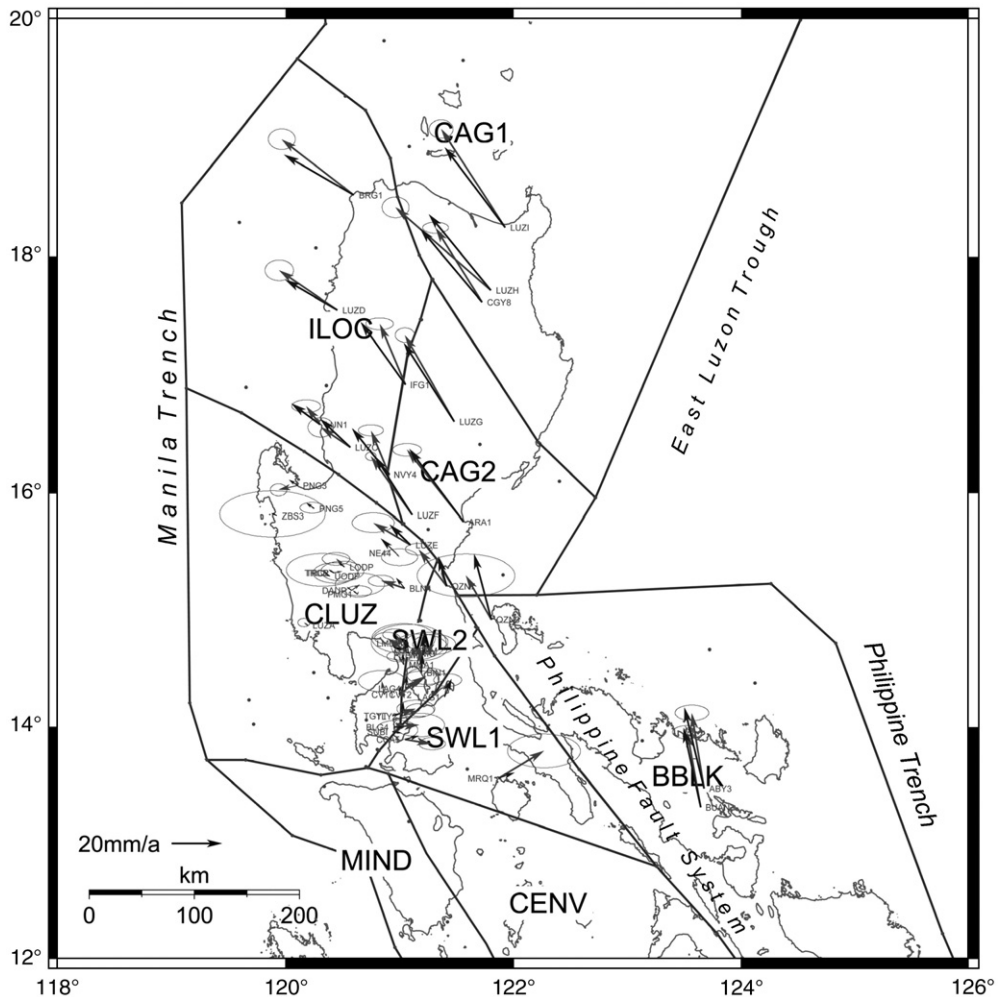


Fig. 6. Observed (arrows with 95% confidence ellipses) and predicted (arrows with no ellipses) GPS-observed site velocities with respect to station MMA8 in block CLUZ from the best-fit model, EH02.

We note that a significant proportion of the surface velocity field results from fault-locking strain, as shown in Fig. 9. Fault-related elastic strain along the Philippine–Digdig–Northern Cordillera fault system is particularly large, due to the high slip rates and coupling coefficients, resulting in significant internal strain within the neighboring blocks.

We obtained Euler poles of rotation that approximate published values (details of the various Euler poles and rotation rates are depicted in Appendix B). The Euler Pole for ILOC–SUND (10.72°N , 118.46°E , $+5.726^\circ/\text{My}$) was comparable with the initial values of 9.34°N , 118.29°E , $+5.478^\circ/\text{My}$ from Rangin et al. (1999). The Euler pole obtained for EURA–PHSP (62.19°N , 169.81°E , $+1.052^\circ/\text{My}$) was also comparable to the values 61.4°N , 163.7°E , $1^\circ/\text{My}$ obtained by Kotake and Kato (2002).

5.2. Coupling along faults and subduction zones

Coupling values for the various block boundaries, derived from the best-fit model EH02, are summarized in Table 8. Based on the resolved coupling values, we can infer that Digdig Fault (near the epicenter of the 1990 Luzon earthquake) is locked to 25 km depth, as well as the southern sections of the Philippine Fault, along the SWL1–BBLK interface. The Northern Cordillera Fault also exhibits high coupling rates at 0.95 ± 0.33 . The Philippine Fault locking value varies, from locked at the south to 0.58 ± 0.10 in central Luzon to around 0.81 ± 0.48 at the ILOC–CLUZ interface in northwestern Luzon. We note that the zone of partial locking is situated near the intersection with the Digdig Fault, suggesting a geometric control. Similarly, the seismically active zones in southwestern Luzon, the Marikina Fault

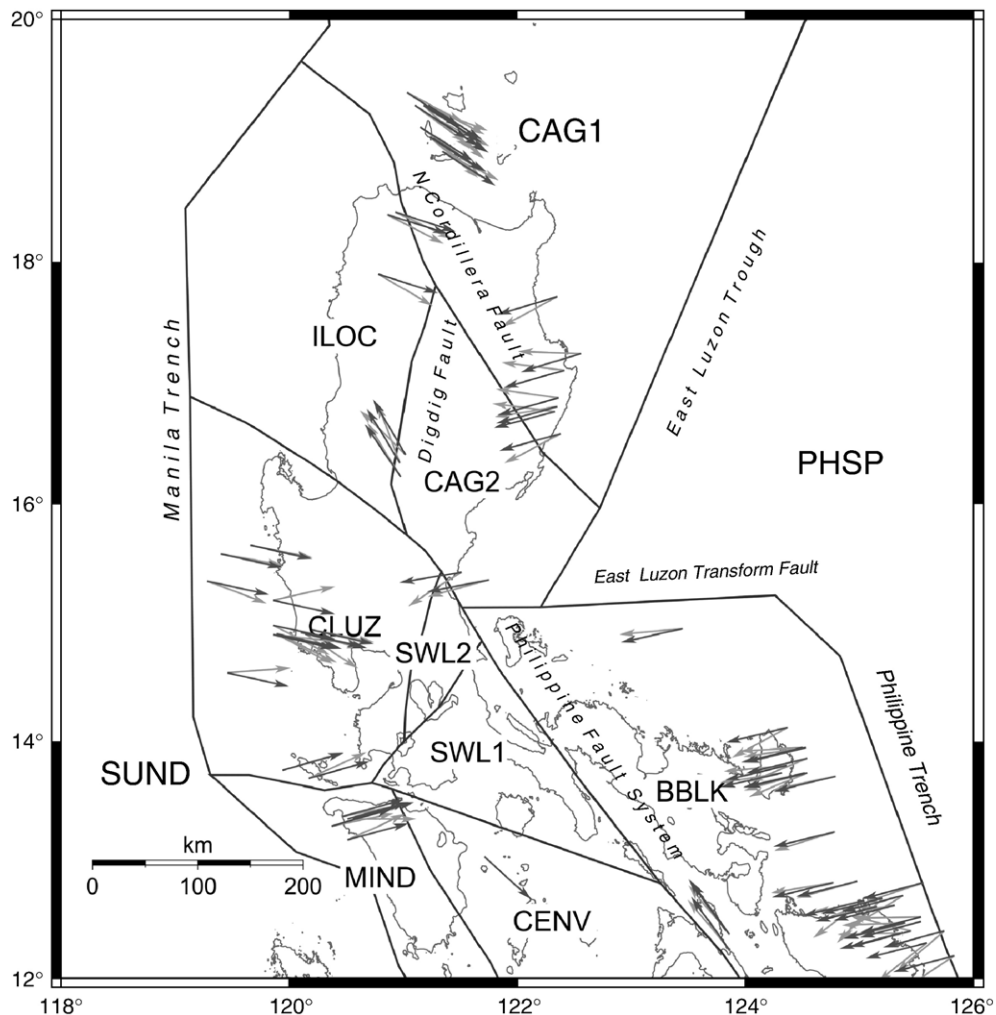


Fig. 7. Observed (light gray arrows) and predicted (black arrows) earthquake slip vectors from the best-fit model, EH02. The 78 earthquake slip vectors were derived from focal mechanisms, through the Harvard CMT Catalogue (1977–2003). Eastward trending slip vectors in CAG1, ILOC, CLUZ and MIND are associated with subduction along the Manila Trench. Westward-trending slip vectors in CAG1 and CAG2 are associated with subduction along the East Luzon Trough, while westward-trending slip vectors at BBLK are associated with subduction at the Manila Trench. Slip vectors that are near the Philippine Fault, Digdig Fault and the Verde Passage–Sibuyan Sea Fault indicate shallow events that are typically strike-slip in nature.

and the Macolod Corridor, were found to be significantly coupled (0.98 ± 0.13 and 0.56 ± 0.31 , respectively). Significantly, the coupling along the Manila Trench subduction zone is inferred to be almost zero. This suggests that, in spite of the very high plate convergence rates revealed in our model, the block motion may result in relatively low seismic potential. This might explain the relative paucity of large-magnitude earthquakes along the Manila Trench margin (Rowlett and Kelleher, 1976; Hamburger et al., 1982). In contrast, the East Luzon Trough appears to be locked (although with relatively high uncertainty). Furthermore, coupling along the Verde Passage Fault was resolved to be 0.84 ± 0.42 on the western side, and 0.37 ± 1.83 on the east (with high

uncertainty). The Philippine Trench exhibits low coupling values at 0.27 ± 0.46 . The paucity of GPS sites in close proximity to the three trenches, however, limits resolution of coupling values along these plate boundaries. In these cases, coupling values may trade off against estimated block convergence rates. Table 8 summarizes coupling values and uncertainty estimates for all the faults and subduction zones.

5.3. Deformation across the Philippine Fault

Our study provides revised estimates of slip rates along the Philippine Fault. We confirm that the Philippine Fault is the main locus of shear deformation within

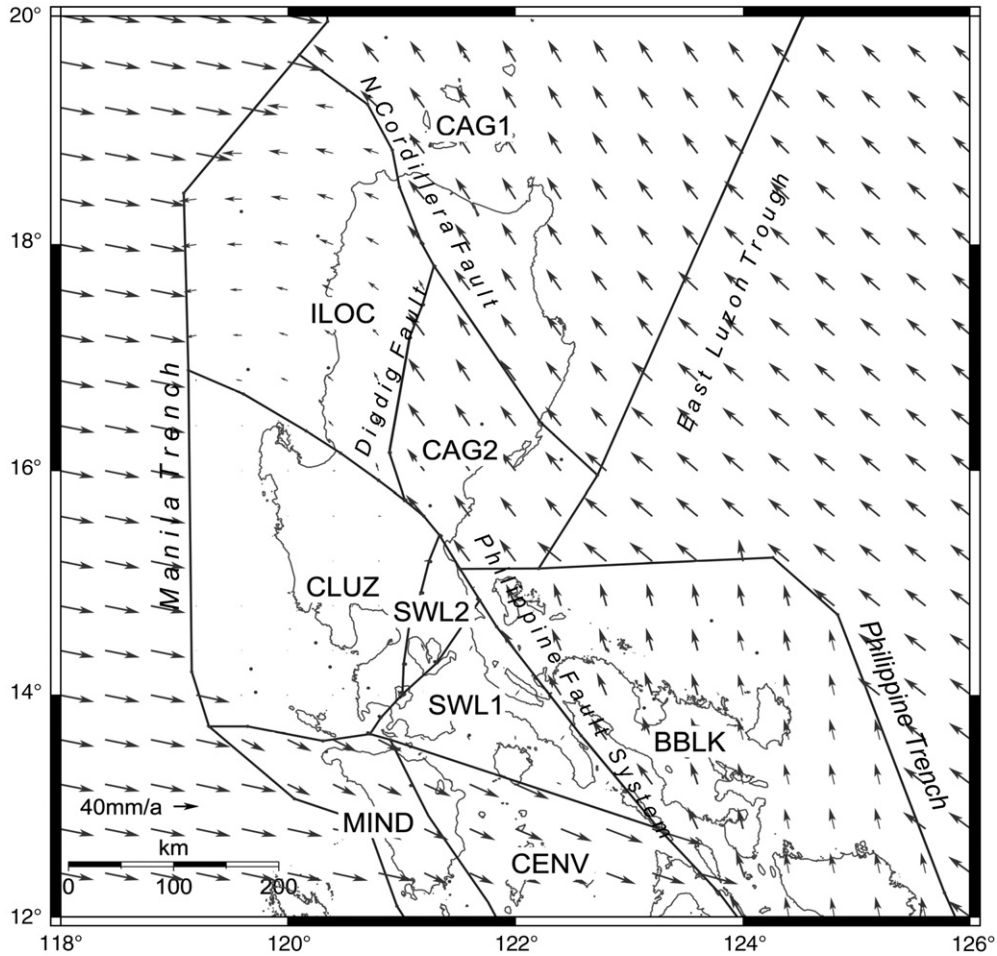


Fig. 8. Total block velocities with respect to block CLUZ based from the best-fit model, EH02. Note that northeastern Luzon, depicted by blocks CAG1 and CAG2, behaves as 1 block, i.e., the Northern Cordillera Fault terminates at the Digdig Fault junction.

Luzon, as suggested by Barrier et al. (1991), Yu et al. (1999) and Rangan et al. (1999). Fig. 10 shows a surface velocity profile across the Philippine Fault. Observed horizontal site velocities (individual points shown in Fig. 10) describe an “s”-pattern across the fault, with the fault-parallel velocities exhibiting more pronounced curvature than the fault-normal component. The fault-parallel component is characteristic of a partially coupled, sinistral strike-slip fault, with a slip rate of $\sim 39.7 \text{ mm yr}^{-1}$. The curved lines on Fig. 10 show modeled velocity distribution when both block rotation and elastic strain associated with fault locking are considered. The breadth of this zone of elastic deformation results from the relatively deep (25 km) locking depth inferred for the fault. Our preferred model indicates fault-parallel slip rates of 29 to 40 mm yr^{-1} , which fall within the ranges proposed by these previous studies.

In contrast, Beavan et al. (2001) proposed a significantly lower long-term slip rate of $\sim 15\text{--}20 \text{ mm yr}^{-1}$. They examined deformation across the Philippine Fault using data from the same geodetic network, but analyzed the long-term slip rate using both an elastic approach and a combined elastic–viscoelastic model. Their values of $\sim 40 \text{ mm yr}^{-1}$ along the northern Philippine Fault obtained using the elastic model correspond well with our estimate. However, they obtained a much lower long-term slip rate, when considering accelerated post-seismic slip following the 1990 Luzon earthquake using the elastic–viscoelastic model. While this rapid post-seismic slip is a viable result of this large crustal earthquake, we conclude for several reasons that the higher rate represents a more reliable long-term slip rate for the central Philippine Fault. First, similar high rates of slip are obtained for neighboring segments of the Philippine Fault that were not affected by the 1990 earthquake. (The

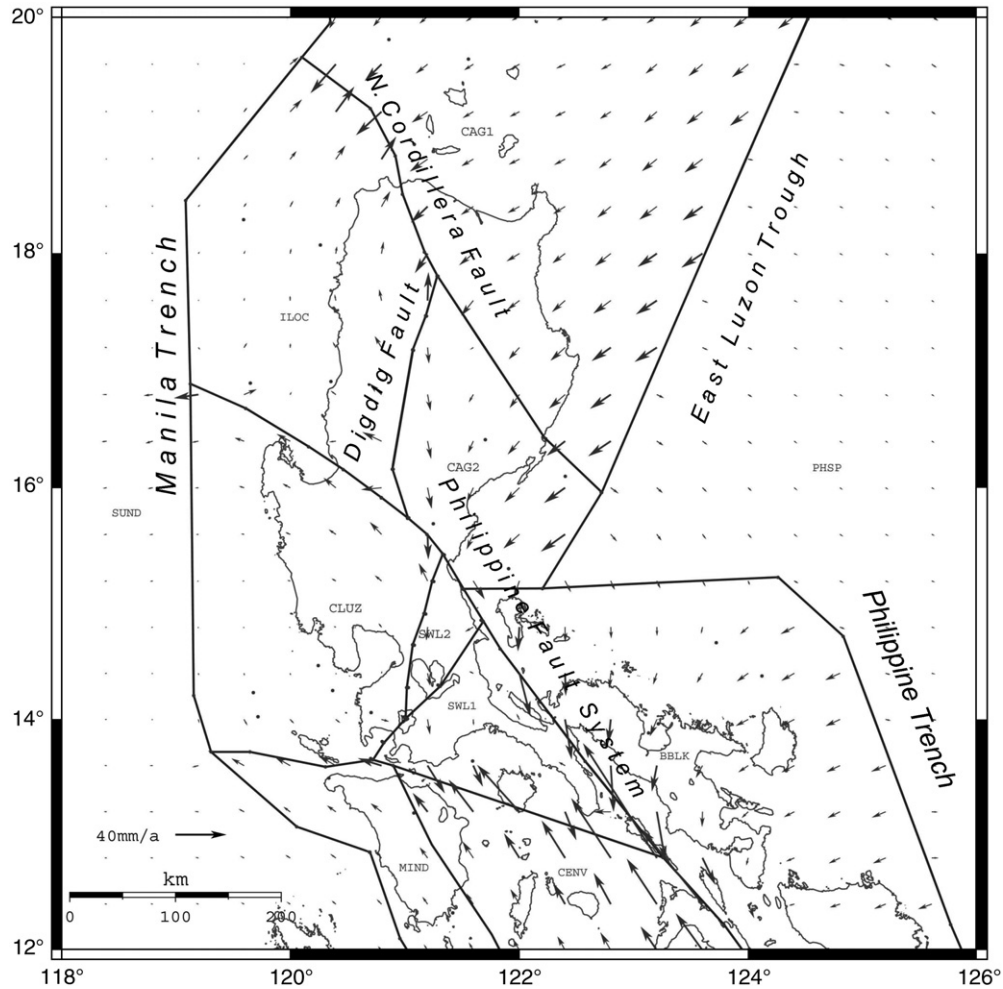


Fig. 9. Fault-locking strain vectors from the best-fit model, EH02. Figure shows large fault-locking strain along the NW–SE trending strike-slip Philippine Fault, the Northern Cordillera Fault and the Philippine Trench/East Luzon Trough.

PF-southern segment moves at about $25\text{--}29\text{ mm yr}^{-1}$, while north of the 1990 epicenter area moves at about $17\text{--}27\text{ mm yr}^{-1}$.) Second, our periodic measurements of site positions show no evidence of significant temporal variations in slip rate, extending as far as twelve years following the main shock. And finally, as discussed in the following section, the long-term recurrence rate for large earthquakes along the Philippine Fault can be readily reconciled with the slip rate when the coupling factor is incorporated in the calculations.

In principle, we can use these fault slip rate estimates, combined with earthquake rupture data, to compute recurrence intervals for large earthquakes. In practice, however, earthquake rupture estimates are only available for the most recent earthquake along the Philippine Fault. The relative block velocities near the northern

areas of the PF (near the Digdig Fault intersection, site of the 1990 M 7.8 event) are estimated at $40\pm 9\text{ mm yr}^{-1}$, and the average dislocation from the 1990 earthquake is $\sim 5.4\text{ m}$ (Yoshida and Abe, 1992). If we consider this to be a characteristic earthquake for this segment of the fault system, we can estimate a recurrence interval of about 111 to 175 years based on the fully coupled elastic model. With partial coupling considered (58% at this segment of the PF), however, the recurrence interval will be much longer (~ 192 to 301 years). This slip rate with partial coupling approaches the paleoseismic recurrence intervals of 300–400 years obtained by Daligdig (1997). Furthermore, the elastic–viscoelastic model explored by Beavan et al. (2001) identifies a long-term slip rate of $15\text{--}20\text{ mm yr}^{-1}$ quite close to the accumulation rates which consider

Table 8

Summary of coupling ratios for the various block boundaries, from the best-fit model, EH02

Fault/subduction zone name	Coupling ratio	Uncertainty (1 σ)
Digdig Fault	1.00	0.11
Macolod Corridor	0.56	0.31
Marikina Fault	0.98	0.13
East Luzon Transform Fault	(0.02)	0.67
Philippine Trench	0.27	0.46
East Luzon Trough	(1.00)	0.62
Manila Trench	0.01	0.18
Phil. Fault-South (BBLK–SWL1)	(1.00)	0.70
Phil. Fault-Middle (CLUZ–CAG2, SWL2–BBLK)	0.58	0.10
Phil. Fault-North (ILOC–CLUZ)	0.81	0.48
Verde Passage–Sibuyan Sea Fault 1 (MIND–CLUZ)	0.84	0.42
Verde Passage–Sibuyan Sea Fault 2 (CENV–SWL1)	(0.37)	(1.83)
Northern Cordillera Fault	0.95	0.33

Values in bold numbers indicate reliable values, while ones in parentheses have high uncertainties (due to low resolution of observations). Coupling ratio is the same and constant at depth, based on the preferred model EH02.

partial coupling (the partially coupled model corresponds to an effective slip rate of 18–28 mm yr⁻¹ or an average rate of 23 mm yr⁻¹). Generalizing these observations, we

can conclude that areas in northern Luzon close to the Philippine and Digdig faults are still exposed to relatively high seismic risk, due to the combination of high coupling values and relatively large fault strain accumulation rates. Areas near the 1990 M 7.8 earthquake (i.e., near the Philippine Fault in north-central Luzon) are clearly at a lower risk due to the short time since its last rupture. Because the last large earthquake occurred only 15 years ago, we may conclude that only about 0.35 m of slip has accumulated since the last earthquake, with an average of 0.25 m of aseismic fault creep. Other segments of the Philippine Fault and Digdig Fault, however, are at higher risk, due to their high strain accumulation rates and coupling rates. Additional concerns might be raised by possible migration of activity to other nearby fault segments, similar to the behavior of other strike-slip systems, such as the Anatolian Fault in Turkey (e.g., Stein et al., 1997).

5.4. The Marikina–Macolod area in southwestern Luzon

Our preferred kinematic model supports the structural interpretations of Förster et al. (1990) and Pubellier et al. (2000), which describe the Macolod Corridor as a complex zone of distributed extension. The hypothesized

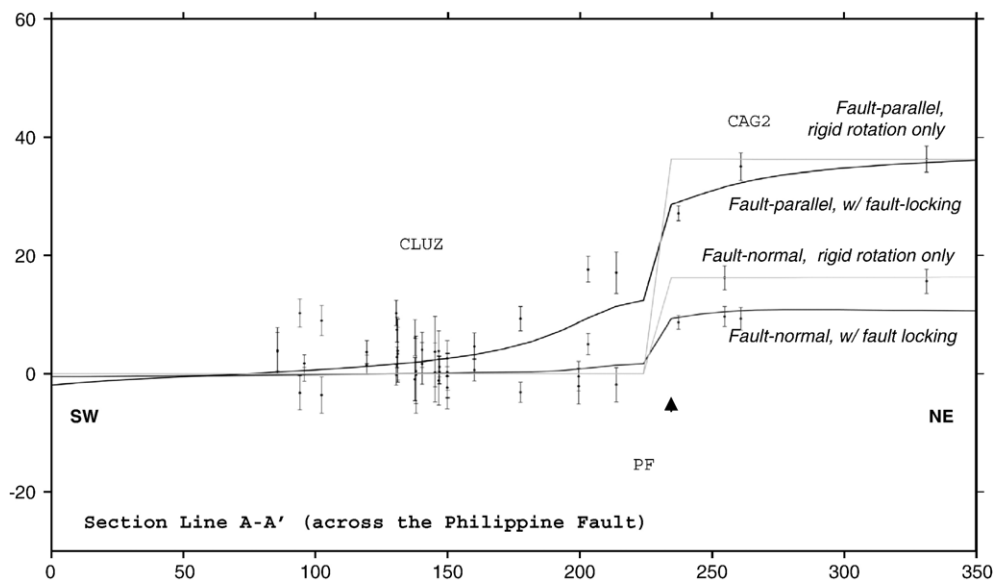


Fig. 10. Modeled elastic strain curves across the Philippine Fault (section line A–A' in Fig. 5), south to north through the CAG2–CLUZ border. Triangle marks location of the fault. The x-axis is the distance along the profile across the fault, while the y-axis is the velocity in mm yr⁻¹. The blue curve represents the model block velocity with fault-locking component parallel to the direction of motion. The cyan line represents the same parallel component with only the rigid block motion (i.e., elastic fault strain excluded). The continuous red line represents the model block velocity with fault-locking component normal to the direction of motion. The pink line represents the same normal component with only the rigid block motion. Blue and red dots represent observed GPS site velocities with error bars (1 sigma) parallel and normal to the fault, respectively. (For interpretation of the references to color in this figure legend, the reader is referred to the web version of this article.)

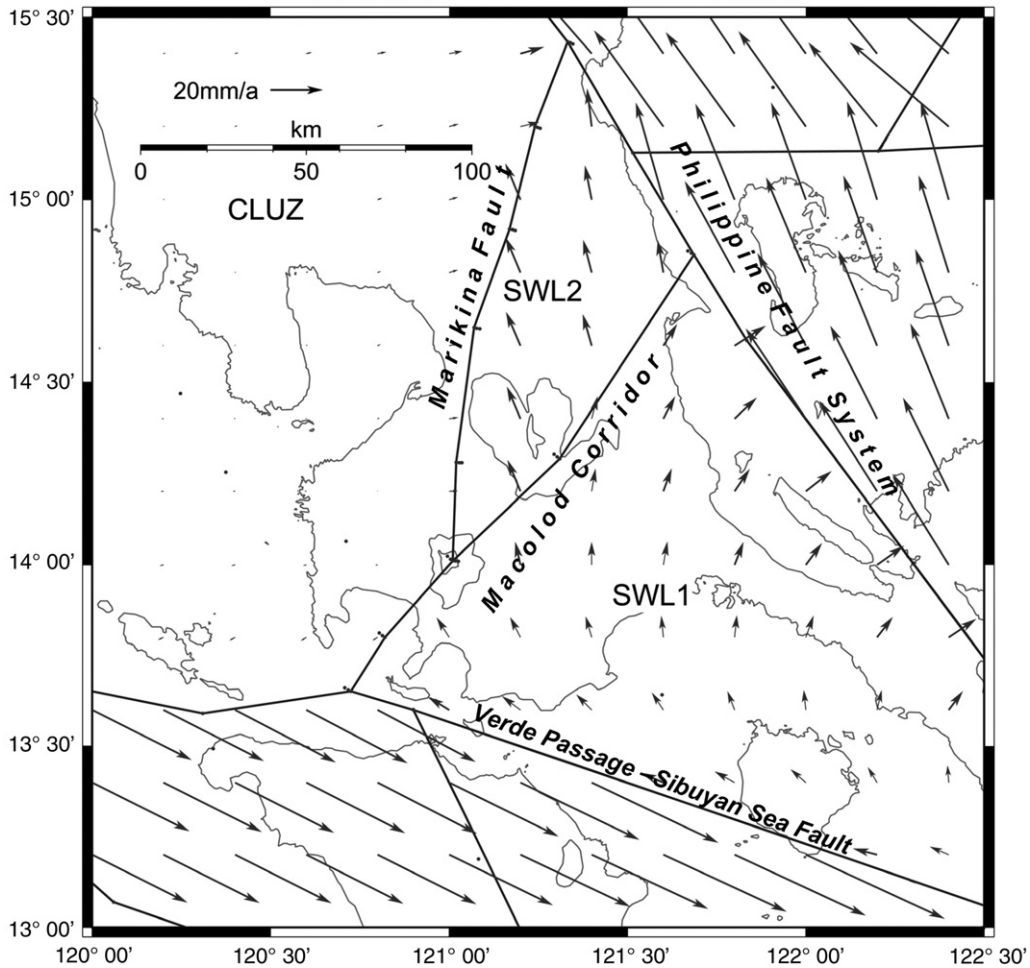


Fig. 11. Detailed model of deformation in the Macolod Corridor area, SW Luzon. Block velocities are derived from the best-fit model (EH02), plotted with respect to block CLUZ. Transpression of about $10\text{--}12\text{ mm yr}^{-1}$ is noted along the Marikina Fault, while $\sim 5\text{--}10\text{ mm yr}^{-1}$ transtensional motion is evident within the Macolod Corridor. Sinistral strike-slip motion of about 40 mm yr^{-1} is also evident at the Verde Passage–Sibuyan Sea Fault.

region of crustal deformation resulting from extension, rotation, crustal thinning, and extensive faulting is verified by our results within the area of the Macolod Corridor, which are shown graphically in Fig. 11. Due to limited geodetic coverage in this area, our study simplifies the Macolod Corridor as a single fault zone, combined with a north–south oriented Marikina fault which intersects the Macolod Corridor near Taal Volcano. Motion along the Marikina Fault is described as oblique, left-lateral strike-slip with a component of compression at $\sim 10\text{--}12\text{ mm yr}^{-1}$ (Table 7). Motion along the Macolod Corridor, meanwhile, is transtensional at $5\text{--}10\text{ mm yr}^{-1}$. Block velocities along the bounding BBLK, MIND and CENV blocks are notably different from CLUZ, SWL1, and SWL2, due to the motions along Verde Passage Fault and the Philippine

Fault. Fault-locking strain increases upon approaching the Philippine Fault northeastward. Both our study and that of Ohkura et al. (2001) find the Macolod area to be rotating, in a counterclockwise sense, with respect to Central Luzon. This rotation is a probable result of the Palawan/Mindoro collision and resulting shear along the Verde Passage fault system. Profiles that cross the Macolod Corridor and the Marikina Fault (Fig. 12) describe a region bounded by multiple faults. The strike-slip component along the Marikina Fault is evident at the left part of Fig. 12, near the 150 km mark. This point is also marked by a downtrend in the fault-normal velocities, typical of compressional motion. The transtensional component along the Macolod Corridor (MACO) is noticeable at the right part of Fig. 12 near the 200 km mark. Elastic curves in this

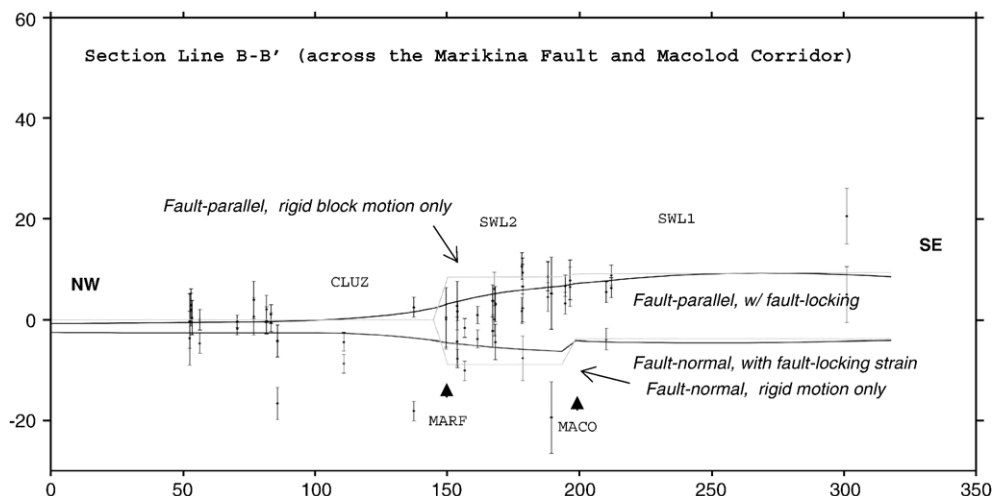


Fig. 12. Elastic strain curve across the Macolod Corridor along an east to west profile (see Fig. 5 for location of transect B–B'). Triangles mark the locations of the Marikina Fault (MARF) and the Macolod Corridor (MACO). Pattern shows typical curves for a normal fault. Descriptions of lines and symbols are the same as in Fig. 10.

area describe a transtensional, strike-slip component at $\sim 5\text{--}10 \text{ mm yr}^{-1}$.

6. Conclusions

Satellite imagery, digital elevation models, and geophysical data are used to define the configuration of active faults and delineation of tectonic blocks that comprise the northern Philippine island arc. We use a combination of earthquake slip vectors and GPS-derived horizontal surface velocities to invert for block rotations and elastic fault strain. We find that the majority of the observed crustal deformation can be explained by block rotations, with a smaller contribution from fault-locking strain. The observed deformation within Luzon requires the contributions of rotations of at least six separate tectonic blocks, delineated by major faults along the boundaries. Based on our inversion tests, we can also conclude that locking depths average at about 25 km, and that coupling rates vary from locked to fully uncoupled for the various faults and subduction zones. Inferred surface velocities confirm that the majority of plate Eurasia–Philippine Sea plate convergence occurs along the western subduction zone, the Manila Trench, with a smaller component contributed by the Philippine Trench and East Luzon Trough. Intraplate deformation in Luzon is dominated by sinistral shear, which is mainly absorbed by the Philippine Fault and its northern splays, the Digdig Fault and the Northern Cordillera Fault.

While the elastic block modeling technique provides a useful first-order characterization of crustal deformation

of Luzon, we recognize that there are still significant limitations to this modeling process. We note the need to characterize and properly incorporate viscoelastic and other time-dependent effects to the model, as post-seismic deformation along the Philippine fault is a likely product of the 1990 earthquake. The spatial resolution of our crustal model for northern Luzon is limited by the density of the geodetic network. Areas of complex surface deformation, such as the Macolod Corridor, easternmost Luzon (BBLK block) and the Ilocos Norte area (ILOC block), where the Philippine Fault separates into numerous splay systems, are obvious candidates for further densification. Expansion of the network into neighboring areas would also be useful, particularly in determining block configurations and motions in areas such as the Mindoro collision zone, the Bicol peninsula, or areas of complex volcano–tectonic interaction. We are confident that improved resolution of tectonic models of the northern Philippines can lead in turn to improvements in the seismic risk models for the Philippines and better understanding of plate boundary zone dynamics.

Acknowledgments

We are grateful to Dr. Renato Solidum and the many able scientists and engineers from the Philippine Institute of Volcanology and Seismology (PHIVOLCS), as well as the National Mapping and Resource Information Authority (NAMRIA), who led the GPS field campaigns described here. In particular, the staff of the PHIVOLCS Volcano Monitoring and Prediction

Division have contributed greatly to this effort. We are particularly indebted to Beth Bartel and Catherine Thibault, who organized much of the GPS data and provided preliminary analyses of the data. We thank Dr. Ronnie Torres of the University of Hawaii for contributing to the DEM work and Dr. Shui-Beih Yu for sharing GPS data collected by the Taiwan Institute of Earth Sciences. UNAVCO provided extensive field support and data archiving that were essential to the success of this project. We further thank the Manila Observatory for sharing satellite data and image processing resources for this collaborative research project. We also thank Sergio Abad II for providing technical assistance on DEM processing, as well as Dr. Emmanuel Ramos, Dr. Mario Aurelio and Jerry Salvador for sharing insights on Luzon geology and tectonics. We thank the USGS, Harvard University and NASA for providing critical data. GMT mapping software (Wessel and Smith, 1998) was used for the preparation of figures. Principal funding for this project was provided by the National Science Foundation Research Grant EAR-0307524. Dr. McCaffrey's participation was supported by the Rensselaer Polytechnic Institute. The comments and suggestions of the two anonymous reviewers and Dr. Mike Sandiford (editor) were indeed valuable in improving the overall content.

Appendix A. Supplementary data

Supplementary data associated with this article can be found, in the online version, at [doi:10.1016/j.tecto.2006.12.001](https://doi.org/10.1016/j.tecto.2006.12.001).

References

- Acharya, H., 1980. Seismic slip on the Philippine Fault and its tectonic implications. *Geology* 8, 40–42.
- Aurelio, M., 2000. Shear partitioning in the Philippines: constraints from Philippine Fault and global positioning system data. *Island Arc* 9, 584–597.
- Bacolcol, T.C., 2003. Etude géodésique de la faille Philippine dans les Visayas, PhD Dissertation, Département de Tectonique, Université Pierre et Marie Curie, Paris Cedex 05, France.
- Barrier, E., Huchon, P., Aurelio, M., 1991. Philippine Fault: a key for Philippine kinematics. *Geology* 19, 32–35.
- Bartel, B., 2002. Magma dynamics at Taal Volcano, Philippines from continuous GPS measurements. Master's Thesis, Department of Geological Sciences, Indiana University, Bloomington, Indiana.
- Bartel, B., Hamburger, M., Meertens, C., Lowry, A., Corpuz, E., 2003. Dynamics of active magmatic and hydrothermal systems at Taal Volcano, Philippines, from continuous GPS measurements. *Journal of Geophysical Research* 108 (B10), 2,475.
- Beavan, J., Silcock, D., Hamburger, M., Ramos, E., Thibault, C., Feir, R., 2001. Geodetic constraints on postseismic deformation following the 1990 Ms 7.8 Luzon Philippines earthquake and implications for Philippine Sea–Eurasian plate motion. *Geochemistry, Geophysics, Geosystems* 2 (200GC000100).
- Bennett, R., Rodi, W., Reilinger, R., 1996. Global positioning system constraints on fault slip rates in southern California and northern Baja, Mexico. *Journal of Geophysical Research* 101 (B10), 21,943–21,960.
- Besana, G., Shibutani, T., Hirano, N., Ando, M., Bautista, B., Narag, I., Punongbayan, R.S., 1995. The shear wave velocity structure of the crust and uppermost mantle beneath Tagaytay, Philippines inferred from receiver function analysis. *Geophysical Research Letters* 22 (23), 3143–3146.
- Bischke, R., Suppe, J., Del Pilar, R., 1990. A new branch of the Philippine fault system as observed from aeromagnetic and seismic data. *Tectonophysics* 183, 243–264.
- Boucher, C., Altamimi, Z., Sillard, P., 1999. The 1997 International Terrestrial Reference Frame (ITRF97). IERS Technical Note, vol. 27. Observatoire de Paris, France.
- Cardwell, R., Isacks, B., Karig, D., 1980. The spatial distribution of earthquakes, focal mechanism solutions, and subducted lithosphere in the Philippine and northeastern Indonesian islands. In: Hayes, D.E. (Ed.), *The Tectonic and Geologic Evolution of Southeast Asian Seas and Islands, Part 1*. The AGU, Geophysical Monograph, vol. 27, pp. 1–35.
- Chamot-Rooke, N., Le Pichon, X., 1999. GPS determined eastward Sundaland motion with respect to Eurasia confirmed by earthquakes slip vectors at Sunda and Philippine Trenches. *Earth and Planetary Science Letters* 173, 439–455.
- Daligdig, J., 1997. Recent faulting and paleoseismicity along the Philippine Fault zone, north central Luzon, Philippines, PhD thesis, faculty of Science, Kyoto University.
- De Boer, J., Odom, L., Ragland, P., Snider, F., Tilford, N., 1980. The Bataan Orogene: eastward subduction, tectonic rotations, and volcanism in the western Pacific (Philippines). *Tectonophysics* 67, 251–282.
- Dziewonski, A.M., Woodhouse, J.H., 1983. An experiment in the systematic study of global seismicity: centroid-moment tensor solutions for 201 moderate and large earthquakes of 1981. *Journal of Geophysical Research* 88, 3,247–3,271.
- Dziewonski, A.M., Chou, T.-A., Woodhouse, J.H., 1981. Determination of earthquake source parameters from waveform data for studies of global and regional seismicity. *Journal of Geophysical Research* 86, 2,825–2,852.
- Fitch, T.J., 1972. Plate convergence, transcurrent faults and internal deformation adjacent to southeast Asia and the western Pacific. *Journal of Geophysical Research* 77, 4,432–4,460.
- Förster, H., Oles, D., Knittel, U., Defant, M., Torres, R., 1990. The Macolod Corridor: a rift crossing the Philippine island arc. *Tectonophysics* 183, 265–271.
- Frey Mueller, J.T., Murray, M.H., Segall, P., Castillo, D., 1999. Kinematics of the Pacific–North America plate boundary zone, northern California. *Journal of Geophysical Research* 104, 7,419–7,441.
- Frey Mueller, J.T., Cohen, S.C., Fletcher, H.J., 2000. Spatial variations in present-day deformation, Kenai Peninsula, Alaska, and their implications. *Journal of Geophysical Research* 105, 8,079–8,107.
- Galgana, G.A., 2005. Kinematics of an active plate boundary zone: insights on the tectonics of Luzon, Philippines using terrain models, focal mechanisms, and GPS observations. Master's Thesis, Department of Geological Sciences, Indiana University, Bloomington, Indiana.
- Gordon, R., Stein, S., 1992. Global tectonics and space geodesy. *Science* 256, 333–342.

- Hamburger, M., Cardwell, R., Isacks, B., 1982. Seismotectonics of the northern Philippine island arc. In: Hayes, D.E. (Ed.), *The Tectonic and Geologic Evolution of Southeast Asian Seas and Islands, Part 2*. The AGU Geophysical Monograph, vol. 27, pp. 1–22.
- Hayes, D., Lewis, S.D., 1984. A geophysical study of the Manila Trench, Luzon, Philippines: 1. Crustal structure, gravity, and regional tectonic evolution. *Journal of Geophysical Research* 89 (B11), 9,171–9,195.
- Houseman, G.A., England, P.S., 1986. Finite strain calculations of continental deformation, 1, Method and general results for convergent zones. *Journal of Geophysical Research* 91, 3,651–3,663.
- Karig, D.E., 1983. Accreted terranes in the northern part of the Philippine archipelago. *Tectonics* 2 (2), 211–236.
- Kotake, Y., Kato, T., 2002. Re-estimation of the relative motion of Philippine Sea plate derived from GPS observations. EOS Transactions, AGU, 83 West Pacific Geophysics Meeting Supplement, Abstract SE31A-19.
- Kennelly, P., Stickney, M., 2000. Using GIS for visualizing earthquake epicenters, hypocenters, faults and lineaments in Montana. U.S. Geological Survey Open-File Report 00-325. <http://pubs.usgs.gov/of/of00-325/kennelly.html>.
- Kreemer, C., Holt, W., Goes, S., Govers, R., 2000. Active deformation in eastern Indonesia and the Philippines from GPS and seismicity data. *Journal of Geophysical Research* 105 (B1), 663–680.
- Kreemer, C., Holt, W., Haines, J., 2003. An integrated global model of present-day plate motions and plate boundary deformation. *Geophysical Journal International* 154 (1), 8–34.
- Larson, K.M., Freymueller, J.T., Philipsen, S., 1997. Global plate velocities from the global positioning system. *Journal of Geophysical Research* 102, 9,961–9,981.
- Leech, D., Treloar, P., Lucas, N., Grocott, J., 2003. Landsat TM analysis of fracture patterns: a case study from the Coastal Cordillera of northern Chile. *International Journal of Remote Sensing* 24 (19), 3,709–3,726.
- Lewis, S., Hayes, D., 1983. The tectonics of northward propagating subduction along eastern Luzon, Philippine Islands. In: Hayes, D.E. (Ed.), *The Tectonic and Geologic Evolution of Southeast Asian Seas and Islands, Part 2*. The AGU Geophysical Monograph, vol. 27, pp. 57–58.
- Lowry, A., Hamburger, M., Meertens, C., Ramos, E., 2001. GPS monitoring of crustal deformation at Taal Volcano, Philippines. *Journal of Volcanology and Geothermal Research* 105, 25–47.
- McCaffrey, R., 1992. Oblique plate convergence, slip vectors, and forearc deformation. *Journal of Geophysical Research* 97, 8,905–8,915.
- McCaffrey, R., 1995. DEF-NODE User's Guide. Rensselaer Polytechnic Institute, Troy.
- McCaffrey, R., 2002. Crustal block rotations and plate coupling. In: Stein, Seth, Freymueller, Jeffrey (Eds.), *Plate Boundary Zones*. AGU Geodynamics Series, vol. 30.
- Michel, G., Yu, Y.Q., Zhu, S.Y., Reigber, Ch., Becker, M., Reinhart, E., Simons, W., Ambrosius, B., Vigny, C., Chamot-Rooke, N., Le Pichon, X., Morgan, P., Matheussen, S., 2001. Crustal motion and block behaviour in SE Asia from GPS measurements. *Earth and Planetary Science Letters* 187, 239–244.
- Morgan, W.J., 1968. Rises, trenches, great faults and crustal blocks. *Journal of Geophysical Research* 73 (6), 1959–1982.
- Ohkura, T., et al., 2001. GPS measurements in the Macolod Corridor, Philippines. *Journal of the Geological Society of the Philippines* 56 (3 and 4), 97–104.
- Okada, Y., 1985. Surface deformation to shear and tensile faults in half-space. *Bulletin of the Seismological Society of America* 75, 1135–1154.
- Pubellier, M., Garcia, F., Loevenbruck, A., Chorowicz, J., 2000. Recent deformation at the junction between the north Luzon block and the central Philippines from ERS-1 images. *Island Arc* 9, 598–610.
- Pubellier, M., Monnier, C., Maury, R., Tamayo, R., 2004. Plate kinematics, origin and tectonic emplacement of supra-subduction ophiolites in SE Asia. *Tectonophysics* 392 (1–4), 9–36.
- Rabus, B., Eineder, M., Roth, A., Bamler, R., 2003. The Shuttle Radar Topography Mission—a new class of digital elevation models acquired by spaceborne radar. *ISPRS Journal of Photogrammetry and Remote Sensing* 57, 241–262.
- Rangin, C., Le Pichon, X., Mazzotti, S., Pubellier, M., Chamot-Rooke, N., Aurelio, M., Walpersdorf, A., Quebral, R., 1999. Plate convergence measured by GPS across the Sundaland/Philippine Sea plate deformed boundary: the Philippines and eastern Indonesia. *Geophysical Journal International* 139, 296–316.
- Rothacher, M., Mervart, L. (Eds.), 1996. *Bernese GPS Software Version 4.0*. Astronomical Institute University of Berne, Berne, Switzerland.
- Rowlett, H., Kelleher, J., 1976. Evolving seismic and tectonic patterns along the western margin of the Philippine Sea plate. *Journal of Geophysical Research* 81 (20), 3518–3524.
- Segall, P., Davis, J., 1997. GPS applications for geodynamics and earthquake studies. *Annual Review of Earth and Planetary Sciences* 25, 301–336.
- Seno, T., Stein, S., Gripp, A., 1993. A model for the motion of the Philippine Sea plate consistent with NUVEL-1 and geological data. *Journal of Geophysical Research* 98, 17,941–17,948.
- Silcock, D., Beavan, J., 2001. Geodetic constraints on coseismic rupture during the 1990 Ms 7.8, Luzon, Philippines, earthquake. *Geochemistry, Geophysics, Geosystems* 2 (7). doi:10.1029/2000GC 000101.
- Smith, W., Sandwell, D., 1997. Global sea floor topography from satellite altimetry and ship depth soundings. *Science* 277, 5334.
- Spakman, W., Nyst, M., 2003. Inversion of relative motion data for estimates of the velocity gradient field and fault slip. *Earth and Planetary Science Letters* 203, 577–591.
- Stein, S., Gordon, R., 1984. Statistical tests of additional plate boundaries from plate motion inversions. *Earth and Planetary Science Letters* 69, 401–412.
- Stein, S., Sella, G., 2002. Plate boundary zones: concept and approaches. *Plate boundary zones*. In: Stein, Seth, Freymueller, Jeffrey (Eds.), *Plate Boundary Zones*. AGU Geodynamics Series, vol. 30, pp. 1–26.
- Stein, R., Barka, A., Dieterich, J., 1997. Progressive failure on the North Anatolian fault since 1939 by earthquake stress triggering. *Geophysical Journal International* 128, 594–604.
- Suppe, J., 1988. Tectonics of arc-continent collision on both sides of the South China Sea; Taiwan and Mindoro. In the Sino-American Symposium on the arc-continent collision and orogenic sedimentation in eastern Taiwan and analogs. *Acta Geologica Taiwanica* 26, 1–18.
- Thatcher, W., 1995. Tectonic block versus continuum description of active tectonic deformation. *Journal of Geophysical Research* 100 (B3), 3,885–3,894.
- Thibault, C., 1999. GPS Measurements of crustal deformation in the northern Philippine Island arc. Master's Thesis, Department of Geological Sciences, Indiana University, Bloomington, Indiana.
- Tomida, M., 1998. Tectonics of Incipient Subduction at the East Luzon Trough, Philippines. Master's Thesis, Department of Geological Sciences, Indiana University, Bloomington, Indiana.
- Torres, R., Mouginiis-Mark, P., Garbeil, H., Bautista, Ramos, E., 2002. Structural analysis of central Luzon, Philippines, using shuttle

- radar topography mission DEM. EOS Transactions, AGU Fall Meeting. abstract #T62C-1318.
- Wallace, L., Beavan, J., McCaffrey, R., Darby, D., 2004. Subduction zone coupling and tectonic block rotations in the North Island, New Zealand. *Journal of Geophysical Research* 109, B12406. doi:10.1029/2004JB003241.
- Wang, Q., Zhang, P.-Z., Freymueller, J.T., et al., 2001. Present-day crustal deformation in China constrained by global positioning system measurements. *Science* 294, 574–577.
- Webb, F.H., Zumberge, J.F., 1993. An Introduction to GIPSY/OASIS II, JPL D-11088. NASA Jet Propulsion Laboratory.
- Wessel, P., Smith, W.H.F., 1998. New, improved version of generic mapping tools released. EOS 79, 579.
- Yoshida, Y., Abe, K., 1992. Source mechanism of the Luzon, Philippines earthquake of July 16, 1990. *Geophysical Research Letters* 19 (6), 545–548.
- Yu, S., Kuo, L., Punongbayan, R., Ramos, E., 1999. GPS observation of crustal deformation in the Taiwan–Luzon region. *Geophysical Research Letters* 26 (7), 923–926.